

Quasi-birth-and-death processes evolving within trees: Applications to comparative phylogenetics

Habtu Kiros Nigus* Barbara R. Holland† Małgorzata M. O’Reilly‡

November 5, 2025

Abstract

We consider a quasi-birth-and-process (QBD) that duplicates itself at some fixed times within a tree that contains information about duplication times and potentially partially observed states. We analyse a continuous trait by discretising it to obtain the QBD level variable. Then, the phase variable is used to model the dynamics of the underlying environment.

Here, we extend the framework of Soewongsono et al. [25] to enable a more general analysis. We develop an efficient recursive algorithm for computing the likelihood of an observed tree under this model and construct several numerical examples to illustrate its application potential. Through our synthetic data examples, we show a range of potential behaviours that could be modelled with this approach. Further, we apply the framework to two empirical examples from comparative phylogenetics (the evolution of range area and body size traits across a phylogeny of 49 mammals) to gain different insights into the evolution of these continuous traits. In this setting duplication of the QBD represents speciation and continuous trait evolution is modelled in a discretised state space. In our empirical examples, we explore the impact of different parameter choices on the corresponding likelihood of observing a given phylogenetic tree and the observed levels at its tips.

Keywords: quasi-birth-and-death processes, trees, Markov chains, matrix-analytic methods, evolution, comparative phylogenetics, likelihood

Mathematics Subject Classification: 60J80, 65C40

1 Introduction

We consider a stochastic process in which a quasi-birth-and-death process (QBD) duplicates itself at some time, and from then on the two copies evolve independently. The information about the evolution

*University of Tasmania, Australia, email: habtukiros.nigus@utas.edu.au

†Australian Research Council Centre of Excellence for Plant Success, University of Tasmania, Australia, email: barbara.holland@utas.edu.au

‡University of Tasmania, Australia, email: malgorzata.oreilly@utas.edu.au

of the resulting family of the QBDs is then recorded in the form of a tree, in which each node corresponds to a duplication, and a branch starts at the time of a duplication event. Suppose that the data in the form of a tree topology with some observable data at the tips is given, which contains the branch lengths. We are interested in finding suitable QBDs that maximise the likelihood of observing the tree and states at the tips of the tree. For an overview of the key results for QBDs in the theory of matrix-analytic methods the reader is referred to Latouche and Ramaswami [18], Neuts [20], Ramaswami [23], He [13], Joyner and Fralix [17], Bean, Pollett and Taylor [3], Bright and Taylor [5], and Phung-Duc et al. [22].

Such a process of duplicating QBDs was previously described by Soewongsono et al. in [25], who used it to study gene duplication and loss within a species tree. In their paper the authors used a specific QBD with a special structure that matched the biological situation of gene duplication, but here we wish to establish more general results that could be applied to a range of problems in queuing theory and comparative phylogenetics. So in this paper, we develop methodology that could be used to model a wide variety of behaviors with QBD parameters fit via numerical optimization.

One area where such a duplicating QBD process could be applied is comparative phylogenetics and this is what motivated the development of this paper. Comparative phylogenetics studies the evolution of traits along an evolutionary tree. Understanding the evolution of traits in phylogenetic trees is crucial for several reasons. It is important for conservation biology, as it helps in designing effective strategies. It helps predict how species might respond to different stresses, such as climate change, habitat fragmentation, or disease spread. Influential models for single continuous traits include the Brownian motion model introduced in this context by Felsenstein [9] and the Ornstein Uhlenbeck (OU) model in Hansen [12] and later in Butler and King [6]. Brownian motion models a trait evolving neutrally, i.e. without directional selection. The OU models are popular for modeling a trait under stabilizing selection, i.e. a trait for which there is some optimal value such that fitness declines as you get further away from the optimum. OU processes have both a stochastic drift component and a deterministic mean-reverting component which moves the trait value towards the optimum at a rate proportional to how far away from the optimum it currently is. More recent papers have investigated models where the trait can evolve according to different regimes in different clades on the evolutionary tree. For example the SURFACE method of Ingram and Mahler [16] considers different OU models operating in different parts of the evolutionary tree. Beaulieu et al [4] expanded the OU model to allow for different drift rates, selection strengths, and trait optima in different parts of the tree. However, these models have faced criticism for being over-parameterized and statistically unidentifiable as noted by Ho and Ané in [14]. QBD models seem to be a promising area to explore further in this context as they provide a flexible structure with phases representing environmental regimes (which could be hidden) and levels corresponding to a trait of interest, thereby allowing modeling of trait evolution in which transition rates may depend on level, phase, or both.

The key contributions of our paper are:

- An approach to modelling the evolution of traits through a duplicating QBD process.
- A novel efficient algorithm for recursive computation of the likelihood of observing a tree, which is more convenient than the algorithm in Soewongsono et al. [25].

- A range of QBD models for the evolution of traits within species and their analysis.
- Application examples to synthetic data that illustrate the modelling potential to a wide range of behaviours and the methodology to draw useful insights from probabilistic metrics, such as drift.
- Applications to two empirical examples from comparative phylogenetics.

This paper is organised as follows. Section 2 introduces the QBD model and details the discretisation of a continuous trait evolving along a single branch. Section 3 describes the algorithms we developed to compute the tree likelihood. In Section 4, we describe a suite of QBDs and discuss the numerical optimisation strategy. In Sections 5 and 6 we present applications of the QBD models to the analysis of synthetic and empirical datasets, respectively, illustrating model performance and biological insights obtained. Finally, in Section 7 we discuss potential directions for future research.

2 Trait evolving along a single branch: QBD model

To model the evolution of a continuous trait of species evolving along a single branch within a phylogenetic tree, as described by Soewongsono et al. in [25], we apply the following approach.

First, assuming that the values of the continuous trait are bounded and have a value between a and b , we discretise the interval $[a, b]$ into levels labelled $n = 0, \dots, N$, so that level $n = 0, \dots, N-1$ corresponds to the interval $[a + \frac{n(b-a)}{N+1}, a + \frac{(n+1)(b-a)}{N+1})$, and level N corresponds to the interval $[a + \frac{N(b-a)}{N+1}, b]$.

Next, we construct a quasi-birth-and-death process (QBD) $\{(X(t), \varphi(t)) : t \geq 0\}$ [13, 18] such that the level variable $X(t)$ represents the level of the trait at time t , while the phase variable $\varphi(t)$ models the underlying factors that control the behavior of the process such as the direction and strength of selection on the trait.

The QBD is a Markov chain process with state space

$$\{(n, i) : n = 0, 1, 2, \dots, N; i = 1, \dots, K\},$$

some initial distribution $\boldsymbol{\alpha} = [\alpha_{(n,i)}]$, $\alpha_{(n,i)} = \mathbb{P}(X(0) = n, \varphi(0) = i)$, and generator

$$\mathbf{Q} = [\mathbf{Q}^{[n,n']}] = \begin{bmatrix} \mathbf{Q}^{[0,0]} & \mathbf{Q}^{[0,1]} & \mathbf{0} & \dots & \dots & \dots & \dots & \mathbf{0} \\ \mathbf{Q}^{[1,0]} & \mathbf{Q}^{[1,1]} & \mathbf{Q}^{[1,2]} & \mathbf{0} & \dots & \dots & \dots & \mathbf{0} \\ \mathbf{0} & \mathbf{Q}^{[2,1]} & \mathbf{Q}^{[2,2]} & \mathbf{Q}^{[2,3]} & \dots & \dots & \dots & \mathbf{0} \\ \vdots & \vdots & \vdots & \vdots & \dots & \dots & \dots & \vdots \\ \mathbf{0} & \mathbf{0} & \mathbf{0} & \mathbf{0} & \dots & \mathbf{Q}^{[N-1,N-2]} & \mathbf{Q}^{[N-1,N-1]} & \mathbf{Q}^{[N-1,N]} \\ \mathbf{0} & \mathbf{0} & \mathbf{0} & \mathbf{0} & \dots & \mathbf{0} & \mathbf{Q}^{[N,N-1]} & \mathbf{Q}^{[N,N]} \end{bmatrix},$$

where matrices $\mathbf{Q}^{[n,n']} = [q_{(n,i)(n',j)}]_{i,j=1,2,\dots,K}$ record transition rates $(n, i) \rightarrow (n', j)$.

We assume that the state space of the QBD is irreducible and so, since the state space of the QBD is finite, there exists the stationary distribution $\boldsymbol{\pi} = [\pi(n, \varphi)]$, $\pi(n, \varphi) = \lim_{t \rightarrow \infty} \mathbb{P}(X(t) = n, \varphi(t) = \varphi)$.

Below, we state the key expressions useful for the evaluation of the distribution at time t summarised in Aksamit, O'Reilly, Palmowski [1]. Suppose that a QBD starts from level n_0 in some phase $i_0 = 1, \dots, K$ according to the initial distribution $\boldsymbol{\alpha} = [\alpha_j]$, $\alpha_j = \mathbb{P}(\varphi(0) = j)$. Then the distribution

at time t vector $\mathbf{f}(t) = [\mathbf{f}_n(t)]_{n=0,1,\dots,N}$ records probabilities $[\mathbf{f}_n(t)]_j = \mathbb{P}\boldsymbol{\alpha}(X_t = n, \varphi(t) = j)$ that the process is in state (n, j) at time t . To evaluate $\mathbf{f}_n(t)$, we may invert the Laplace Transforms $[\tilde{\mathbf{f}}_n(s)]_j = \int_0^\infty e^{-st} \mathbb{P}\boldsymbol{\alpha}(X_t = n, \varphi(t) = j) dt$ using standard numerical inversion algorithms (see e.g. Den Iseger [7] or Horvath et al. [15]), by applying

$$\begin{aligned}\tilde{\mathbf{f}}_{n_0}(s) &= -\boldsymbol{\alpha} \left((\mathbf{Q}^{[n_0, n_0]} - s\mathbf{I}) + \widehat{\mathbf{R}}^{(n_0-1)}(s) \mathbf{Q}^{[n_0-1, n_0]} + \widetilde{\mathbf{R}}^{(n_0+1)}(s) \mathbf{Q}^{[n_0+1, n_0]} \right)^{-1} \\ \tilde{\mathbf{f}}_n(s) &= -\boldsymbol{\alpha} \mathbf{H}^{n_0, n}(s) \left((\mathbf{Q}^{[n, n]} - s\mathbf{I}) + \widehat{\mathbf{R}}^{(n-1)}(s) \mathbf{Q}^{[n-1, n]} + \widetilde{\mathbf{R}}^{(n+1)}(s) \mathbf{Q}^{[n+1, n]} \right)^{-1}, \quad n > n_0, \\ \tilde{\mathbf{f}}_n(s) &= -\boldsymbol{\alpha} \mathbf{G}^{n_0, n}(s) \left((\mathbf{Q}^{[n, n]} - s\mathbf{I}) + \widehat{\mathbf{R}}^{(n-1)}(s) \mathbf{Q}^{[n-1, n]} + \widetilde{\mathbf{R}}^{(n+1)}(s) \mathbf{Q}^{[n+1, n]} \right)^{-1}, \quad n < n_0\end{aligned}$$

where

$$\begin{aligned}\widetilde{\mathbf{R}}^{(n)}(s) &= -\mathbf{Q}^{[n-1, n]} (\mathbf{Q}^{[n, n]} - s\mathbf{I} + \widetilde{\mathbf{R}}^{(n+1)}(s) \mathbf{Q}^{[n+1, n]})^{-1}, \quad \widetilde{\mathbf{R}}^{(N+1)}(s) = \mathbf{0}, \\ \widehat{\mathbf{R}}^{(n)}(s) &= -\mathbf{Q}^{[n+1, n]} (\widehat{\mathbf{R}}^{(n-1)}(s) \mathbf{Q}^{[n-1, n]} + \mathbf{Q}^{[n, n]} - s\mathbf{I})^{-1}, \quad \widehat{\mathbf{R}}^{(-1)}(s) = \mathbf{0},\end{aligned}$$

and, for any k such that $n+1 \leq n+k \leq N$,

$$\begin{aligned}\mathbf{H}^{n, n+k}(s) &= \mathbf{H}^{n, n+1}(s) \mathbf{H}^{n+1, n+2}(s) \times \dots \times \mathbf{H}^{n+k-1, n+k}(s), \\ \mathbf{H}^{n, n+1}(s) &= -(\mathbf{Q}^{[n, n]} - s\mathbf{I} + \mathbf{Q}^{[n, n-1]} \mathbf{H}^{n-1, n}(s))^{-1} \mathbf{Q}^{[n, n+1]}, \quad \mathbf{H}^{-1, 0}(s) = \mathbf{0},\end{aligned}$$

and, for any k such that $0 \leq n-k \leq n-1$,

$$\begin{aligned}\mathbf{G}^{n, n-k}(s) &= \mathbf{G}^{n, n-1}(s) \mathbf{G}^{n-1, n-2}(s) \times \dots \times \mathbf{G}^{n-k+1, n-k}(s), \\ \mathbf{G}^{n, n-1}(s) &= -(\mathbf{Q}^{[n, n]} - s\mathbf{I} + \mathbf{Q}^{[n, n+1]} \mathbf{G}^{n+1, n}(s))^{-1} \mathbf{Q}^{[n, n-1]}, \quad \mathbf{G}^{N+1, N}(s) = \mathbf{0}.\end{aligned}$$

3 Likelihood of observing certain traits at the tips of a phylogenetic tree: Algorithmic approach

We develop a methodology for the computation of the likelihood of the phylogenetic tree, given the tree topology with branch lengths and trait values observed at the tips. In the initial Algorithm 1, built on the ideas developed by Soewongsono et al. in [25], we assume that distance from the root of the tree to each tip is the same for all tips. This implies the tree is clock-like. In the phylogenetics literature this is referred to as the ultrametric condition. In the improved Algorithm 2, we remove this assumption, and also develop a more general idea, leading to a more convenient computation.

3.1 Algorithm 1

First, consider a simple motivating example: a phylogenetic tree with two branches, each of length t , that started with a branching event at time $t_B < t$. To model this, assume a QBD with initial distribution row vector $\mathbf{f}(t_B)$. Suppose that we observe trait levels n_L and n_R at the left and right tip of the tree, respectively. Then the corresponding likelihood is,

$$\mathbf{f}(t_B) \times \left((\mathbf{P}_{n_L}(t - t_B) \times \mathbf{1}) \odot (\mathbf{P}_{n_R}(t - t_B) \times \mathbf{1}) \right), \quad (1)$$

where $\mathbf{1}$ is a column vector of ones and $\mathbf{P}(t)$ is the conditional distribution matrix at time t ,

$$\mathbf{P}(t) = [P_{(n,i),(n',j)}(t)]_{n,n'=0,\dots,N;i,j=1,\dots,K} \quad (2)$$

such that the $(n, i), (n', j)$ entry of $\mathbf{P}(t)$ is given by

$$P_{(n,i),(n',j)}(t) = \mathbb{P}(X(t) = n', \varphi(t) = j \mid X(0) = n, \varphi(0) = i), \quad (3)$$

and for any m (e.g. $m = n_L$ or $m = n_R$),

$$\mathbf{P}_m(t) = [P_{(n,i),(n',j)}(t)]_{n'=m,n=0,\dots,N;i,j=1,\dots,K} \quad (4)$$

is a matrix collecting the conditional probabilities corresponding to observing trait level m at time t .

Note that $(\mathbf{P}_{n_L}(t - t_B) \times \mathbf{1}) \odot (\mathbf{P}_{n_R}(t - t_B) \times \mathbf{1})$ is a column vector recording the conditional likelihood of observing the traits n_L and n_R at the same time t , and so (1) is a scalar.

We generalise the above idea to the recursive formula for the likelihood of the phylogenetic tree as follows. Denote by $f(T^*; (t_1, \dots, t_B); t)$ the (scalar) likelihood of the tree T^* with $B + 1$ different species and branching events at times t_1, \dots, t_B respectively, that occurred before the current time t . Further, denote by $\mathbf{f}(T^{*(k,b)}(t_b, t))$ the conditional (row vector) likelihood of the (k, b) -th subtree that starts at time t_b , $b = 0, \dots, B$, and ends at time t , counting $k = 0, 1, \dots, b$ from the left to the right on the tree, see Figure 1.

We then have the following recursive formula,

$$f(T^*; (t_1, \dots, t_B); t) = \mathbf{f}(t_1) \times \left(\mathbf{f}(T^{*(0,1)}(t_1, t)) \odot \mathbf{f}(T^{*(1,1)}(t_1, t)) \right), \quad (5)$$

where, for $b = 1, \dots, B - 1$, assuming that the speciation at time t_b occurs on the ℓ_b -th subtree $T^{*(\ell_b, b-1)}$ for some $\ell_b = 0, \dots, b - 1$,

$$\mathbf{f}(T^{*(k,b)}(t_b, t)) = \begin{cases} \mathbf{P}(t_{b+1} - t_b) \times \mathbf{f}(T^{*(k,b+1)}(t_{b+1}, t)) & k < \ell_b, \\ \left(\mathbf{P}(t_{b+1} - t_b) \times \mathbf{f}(T^{*(k,b+1)}(t_{b+1}, t)) \right) \\ \odot \left(\mathbf{P}(t_{b+1} - t_b) \times \mathbf{f}(T^{*(k+1,b+1)}(t_{b+1}, t)) \right) & k = \ell_b, \\ \mathbf{P}(t_{b+1} - t_b) \times \mathbf{f}(T^{*(k+1,b+1)}(t_{b+1}, t)) & k > \ell_b, \end{cases} \quad (6)$$

and

$$\mathbf{f}(T^{*(k,B)}(t_B, t)) = \begin{cases} \mathbf{P}_{m(k,B)}(t - t_B) \times \mathbf{1} & k < \ell_B, \\ \left(\mathbf{P}_{m(k,B)}(t - t_B) \times \mathbf{1} \right) \odot \left(\mathbf{P}_{m(k+1,B)}(t - t_B) \times \mathbf{1} \right) & k = \ell_B, \\ \mathbf{P}_{m(k+1,B)}(t - t_B) \times \mathbf{1} & k > \ell_B, \end{cases} \quad (7)$$

where $m(k, B)$ is the level (trait) observed at the k -th leftmost tip of the phylogenetic tree with B branching events at times t_1, \dots, t_B and a root at time t_0 .

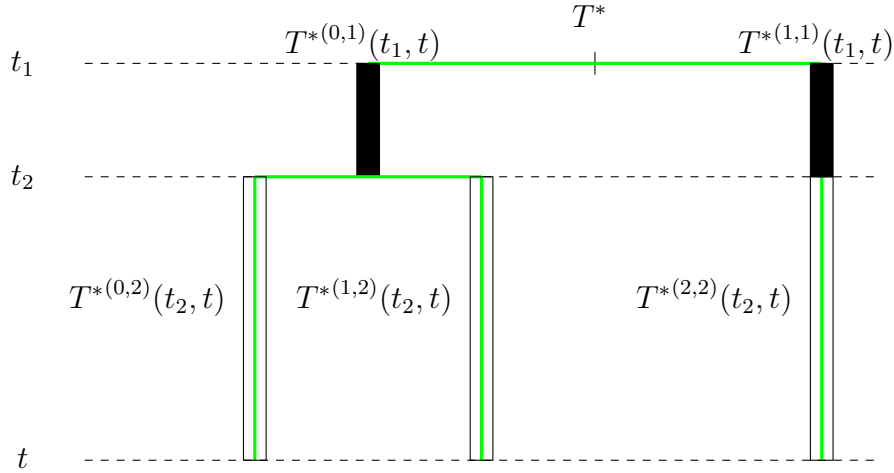


Figure 1: Species tree T^* (figure adapted from Soewongsono et al. [25] to the model considered here). Branching event at time t_1 results in two subtrees, $T^{*(0,1)}(t_1, t)$ and $T^{*(1,1)}(t_1, t)$. Next, another branching event occurs at time t_2 , which results in two subtrees of $T^{*(0,1)}(t_1, t)$, being $T^{*(0,2)}(t_2, t)$ and $T^{*(1,2)}(t_1, t)$, respectively. The corresponding part of the $T^{*(1,1)}(t_1, t)$ that starts at time t_2 is denoted $T^{*(2,2)}(t_2, t)$.

3.2 Algorithm 2

The required input to Algorithm 1 is the information about the speciation times t_1, \dots, t_B , the ordering of the subtrees $(T^{*(k,b)}(t_b, t))$ for $k = 0, \dots, b$, and the assumption is that all external branches terminate at the same time t . Since trees in which external branches may terminate at different times often occur, for example, in datasets where we have information on trait values for fossils, we may remove this assumption and rewrite (7) as

$$\mathbf{f}(T^{*(k,B)}(t_N, t)) = \begin{cases} \mathbf{P}_{m(k,B)}(b_k) \times \mathbf{1} & k < \ell_N, \\ (\mathbf{P}_{m(k,B)}(b_k) \times \mathbf{1}) \odot (\mathbf{P}_{m(k+1,B)}(b_{k+1}) \times \mathbf{1}) & k = \ell_B, \\ \mathbf{P}_{m(k+1,N)}(b_k) \times \mathbf{1} & k > \ell_B, \end{cases} \quad (8)$$

where we additionally assume that b_k is the full length of the external branch k , rather than the length $(t - t_B)$ of its part from the most recent speciation event on the tree at time t_B , unlike in Algorithm 1.

Furthermore, it is more convenient to represent the input in a format in which we record the parent nodes, the children nodes, the connections between the various nodes, and the distances between them. For example, the topology of the tree in Figure 3 corresponding to data discussed later in Section 5, can

be represented in a matrix form as

Parent node	Child node	Distance
5	1	1
5	2	1
6	5	1
6	3	2
7	6	1
7	4	3

(9)

where parent node 5 points at child 1, with the distance between them being 1, and so on.

Therefore, in our improved Algorithm 2, using the input matrix such as in (9), we follow these steps.

- (1) First, for each tip of the phylogenetic tree, evaluate the column vector recording the conditional likelihood of observing the trait level at that tip, given the distribution of the phases at the start of the corresponding branch.
- (2) Next, for each pair of the tips with the same parent, take Hadamard product of their column vectors, resulting in one column vector for each such pair.
- (3) Further, left-multiply each column vector by a conditional probability matrix corresponding to the branching event directly above, resulting in a column vector again.
- (4) Repeat (2) until left with two column vectors. Take their Hadamard product and left-multiply by the initial distribution (row vector) of phases at the parent node.

So, rather than perform recursive computations for each subinterval (t_{b-1}, t_b) as in (6), in this improved Algorithm 2, we perform computations for each branch considering its full length, similarly to the approach applied to a different Markov model by Felsenstein in [8].

Now, denote by $t(k)$ the time corresponding to node k at which a speciation occurs, resulting in two subtrees, the left subtree $T_L^*(k)$ and the right subtree $T_R^*(k)$, with corresponding likelihoods $\mathbf{f}(T_L^*(k))$ and $\mathbf{f}(T_R^*(k))$ respectively. Also, denote by $c_L(k)$ and $c_R(k)$, the two children of node k , being the nodes below k on the left and the right subtree, respectively. Further, let $d(c, p)$ be the distance between child node c and its parent p (the length of the branch that starts at parent node p and terminates at child node c), see Figure 2.

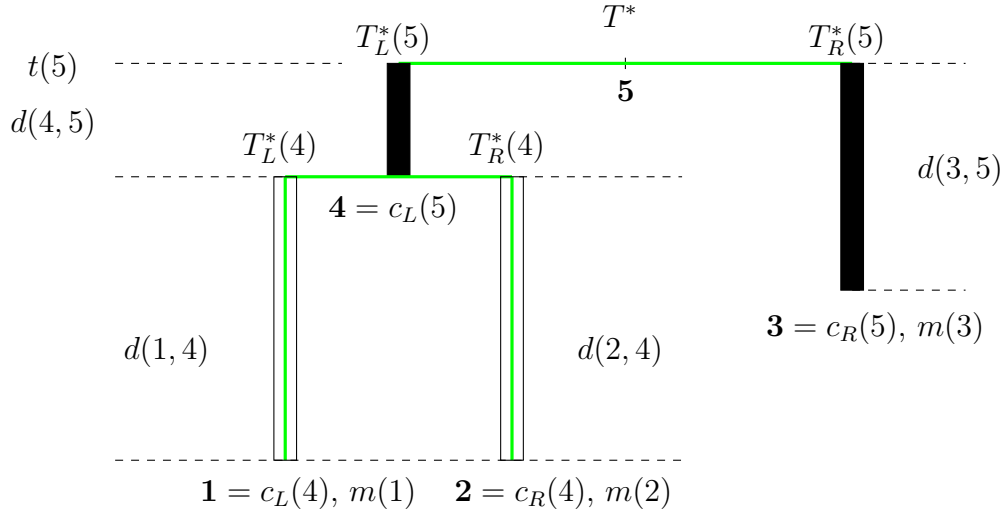


Figure 2: Species tree T^* (notation in Algorithm 2): The tree starts at time $t(5)$ with parent node 5 who has (left and right) children nodes $4 = c_L(5)$ and $3 = c_R(5)$. Nodes 1, 2, and 3 are the tips of the tree, with $1 = c_L(4)$ and $2 = c_R(4)$ being the (left and right) children nodes of their parent node 4. Trait levels $m(1)$, $m(2)$ and $m(3)$ are observed at tips 1, 2, and 3, respectively. Tip 3 is some fossil record.

Then, the recursive formula for Algorithm 2 is written as,

$$f(T^*; p) = \mathbf{f}(t(p)) \times (\mathbf{f}(T_L^*(p)) \odot \mathbf{f}(T_R^*(p))), \quad (10)$$

where p is the parent node at the root of the tree corresponding to branching event at time $t(p)$, and for any subtree $T_\bullet^*(k)$, $\bullet = L, R$, corresponding to an internal node k ,

$$\mathbf{f}(T_\bullet^*(k)) = (\mathbf{P}(d(c_\bullet(k), k)) \times \mathbf{f}(T_L^*(c_\bullet(k))) \odot (\mathbf{P}(d(c_\bullet(k), k)) \times \mathbf{f}(T_R^*(c_\bullet(k)))) \quad (11)$$

whenever $c_\bullet(k)$ is also an internal node, and

$$\mathbf{f}(T_\bullet^*(k)) = \mathbf{P}_{m(c_\bullet(k))}(d(c_\bullet(k), k)) \times \mathbf{1} \quad (12)$$

whenever $c_\bullet(k)$ is one of the tips of the tree and $m(c_\bullet(k))$ is the trait level observed at that tip.

In the practical application of the recursive formula for Algorithm 2, we evaluate the quantities in the direction from the tips to the root of the tree. For example, to evaluate the likelihood of the tree depicted in Figure 2, we first evaluate the likelihoods of the two (left and right) subtrees starting from the internal node 4,

$$\mathbf{f}(T_L^*(4)) = \mathbf{P}_{m(1)}(d(1, 4)) \times \mathbf{1}, \quad \mathbf{f}(T_R^*(4)) = \mathbf{P}_{m(2)}(d(2, 4)) \times \mathbf{1}$$

then the two (left and right) subtrees starting from the internal node 5,

$$\mathbf{f}(T_L^*(5)) = \mathbf{P}(d(4, 5)) \times (\mathbf{f}(T_L^*(4)) \odot \mathbf{f}(T_R^*(4))), \quad \mathbf{f}(T_R^*(5)) = \mathbf{P}_{m(3)}(d(3, 5)) \times \mathbf{1},$$

and finally,

$$\mathbf{f}(T^*; 5) = \mathbf{f}(t(5)) \times (\mathbf{f}(T_L^*(5)) \odot \mathbf{f}(T_R^*(5))).$$

Remark 1 We note that our algorithm can be readily modified to include information about the internal nodes by replacing block matrices $\mathbf{P}_{m(c_\bullet(k))}(d(c_\bullet(k), k))$ with a suitable range of columns.

Model	Number of Phases	$\mathbf{Q}^{[n,n+1]}$	$\mathbf{Q}^{[n,n-1]}$	$\mathbf{Q}^{[n,n]}$
QBD0	2	$\begin{bmatrix} \lambda/2 & \lambda/2 \\ 0 & 0 \end{bmatrix}$	$\begin{bmatrix} 0 & 0 \\ \mu/2 & \mu/2 \end{bmatrix}$	$\begin{bmatrix} -\lambda & 0 \\ 0 & -\mu \end{bmatrix}$
QBD1	3	$\begin{bmatrix} 0 & \lambda_1 & \lambda_2 \\ 0 & 0 & 0 \\ \lambda_3 & 0 & 0 \end{bmatrix}$	$\begin{bmatrix} 0 & 0 & 0 \\ \mu/3 & \mu/3 & \mu/3 \\ 0 & 0 & 0 \end{bmatrix}$	$\begin{bmatrix} -(\lambda_1 + \lambda_2) & 0 & 0 \\ 0 & -\mu & 0 \\ 0 & 0 & -\lambda_3 \end{bmatrix}$
QBD2	4	$\begin{bmatrix} 0 & \lambda_1 & \lambda_2 & \lambda_3 \\ 0 & 0 & 0 & 0 \\ \lambda_4 & \lambda_5 & 0 & 0 \\ 0 & 0 & 0 & 0 \end{bmatrix}$	$\begin{bmatrix} 0 & 0 & 0 & 0 \\ \mu_1 & 0 & \mu_2 & \mu_3 \\ 0 & 0 & 0 & 0 \\ \mu_4 & \mu_5 & 0 & 0 \end{bmatrix}$	$\begin{bmatrix} -(\lambda_1 + \lambda_2 + \lambda_3) & 0 & 0 & 0 \\ 0 & -(\mu_1 + \mu_2 + \mu_3) & 0 & 0 \\ 0 & 0 & -(\lambda_4 + \lambda_5) & 0 \\ 0 & 0 & 0 & -(\mu_4 + \mu_5) \end{bmatrix}$
QBD3	5	$\begin{bmatrix} r_1 & r_1 & r_1 & r_1 & r_1 \\ r_2 & r_2 & r_2 & r_2 & r_2 \\ 0 & 0 & 0 & 0 & 0 \\ 0 & 0 & 0 & 0 & 0 \\ 0 & 0 & 0 & 0 & 0 \end{bmatrix}$	$\begin{bmatrix} 0 & 0 & 0 & 0 & 0 \\ 0 & 0 & 0 & 0 & 0 \\ r_3 & r_3 & r_3 & r_3 & r_3 \\ r_4 & r_4 & r_4 & r_4 & r_4 \\ 0 & 0 & 0 & 0 & 0 \end{bmatrix}$	$\begin{bmatrix} -(5r_1) & 0 & 0 & 0 & 0 \\ 0 & -(5r_2) & 0 & 0 & 0 \\ 0 & 0 & -(5r_3) & 0 & 0 \\ 0 & 0 & 0 & -(5r_4) & 0 \\ r_5 & r_6 & r_7 & r_8 & -(r_5 + r_6 + r_7 + r_8) \end{bmatrix}$
QBD4	5	$\begin{bmatrix} \alpha r_1 & (1-\alpha)r_1 & 0 & 0 & 0 \\ (1-\alpha)r_2/2 & \alpha r_2 & (1-\alpha)r_2/2 & 0 & 0 \\ 0 & 0 & 0 & 0 & 0 \\ 0 & 0 & 0 & 0 & 0 \\ 0 & 0 & 0 & 0 & 0 \end{bmatrix}$	$\begin{bmatrix} 0 & 0 & 0 & 0 & 0 \\ 0 & 0 & 0 & 0 & 0 \\ 0 & 0 & 0 & 0 & 0 \\ 0 & 0 & (1-\alpha)r_4/2 & \alpha r_4 & (1-\alpha)r_4/2 \\ 0 & 0 & 0 & (1-\alpha)r_5 & \alpha r_5 \end{bmatrix}$	$\begin{bmatrix} -r_1 & 0 & 0 & 0 & 0 \\ 0 & -r_2 & 0 & 0 & 0 \\ 0 & (1-\beta)r_3 & -r_3 & \beta r_3 & 0 \\ 0 & 0 & 0 & -r_4 & 0 \\ 0 & 0 & 0 & 0 & -r_5 \end{bmatrix}$

Table 1: Summary of QBD models and their associated block matrices. Each model defines transition dynamics across discrete levels and phases. The matrix $\mathbf{Q}^{[n,n+1]}$ governs transitions to the next higher level, while $\mathbf{Q}^{[n,n-1]}$ governs transitions to the next lower level. Rows correspond to phases at the current level, and columns to phases at the destination level.

4 Numerical Examples: QBD models

Below, we present several examples to illustrate the application of our methodology for computing the likelihood of observing the phylogenetic species tree given its topology and trait values observed at its tips. In the examples of the QBD models considered in this section, we assume that the block matrices $\mathbf{Q}^{[n,n+1]}$, $\mathbf{Q}^{[n,n-1]}$, and $\mathbf{Q}^{[n,n]}$ are the same for all $n = 1, \dots, N-1$, and that $\mathbf{Q}^{[0,0]} = \mathbf{Q}^{[n,n]} + \mathbf{Q}^{[n,n-1]}$ and $\mathbf{Q}^{[N,N]} = \mathbf{Q}^{[n,n]} + \mathbf{Q}^{[n,n+1]}$, with $N = 100$.

Let $\boldsymbol{\xi}$ be the stationary distribution of the Markov chain with generator $\mathbf{A} = \mathbf{Q}^{[n,n+1]} + \mathbf{Q}^{[n,n-1]} + \mathbf{Q}^{[n,n]}$. Denote by

$$\gamma = \boldsymbol{\xi} \mathbf{Q}^{[n,n+1]} \mathbf{1} - \boldsymbol{\xi} \mathbf{Q}^{[n,n-1]} \mathbf{1} \quad (13)$$

the drift measure of the QBD, which can be positive, negative, or zero. Positive drift $\gamma > 0$ indicates the tendency of the trait to increase, while negative drift $\gamma < 0$ indicates the tendency of the trait to decrease, in the long-run. Zero drift $\gamma = 0$ indicates no tendency to increase or decrease in the long run.

In all examples, to fit model parameters, we use the following three methods: manual (trial and error), Nelder-Mead, and Broyden-Fletcher-Goldfarb-Shanno (BFGS) algorithm, see Section 4.2.

4.1 Description of QBD Models (Table 1)

A simple QBD with two phases (QBD0), as shown in Table 1, models random transitions between two states. The level increases at rate λ when the process is in phase 1 and decreases at rate μ when in phase 2. When $\lambda = \mu$, this model exhibits zero drift and is intended to be a discrete analogue of Brownian motion.

QBD1 has three phases with both upward and downward transitions. At level n , the process in phase 1 may increase to level $n + 1$, transitioning to phase 2 or phase 3 at rates λ_1 and λ_2 , respectively. Conversely, a process in phase 3 at level n can increase to level $n + 1$ in phase 1 at rate λ_3 . Downward transitions occur from phase 2, where the process moves to level $n - 1$ in any of the three phases with equal probability, each at rate $\mu/3$.

QBD2 extends the structure of QBD1 by introducing a fourth phase. At level n , a process in phase 1 can transition to level $n + 1$, entering phase 2, phase 3, or phase 4 at rates λ_1 , λ_2 , and λ_3 , respectively. Similarly, a process in phase 3 at level n can transition upward to phase 1 or phase 2 at rates λ_4 and λ_5 . Downward transitions occur from phase 2, where the process moves to level $n - 1$, entering phase 1, phase 3, or phase 4 at rates μ_1 , μ_2 , and μ_3 , respectively.

QBD3 has five phases with two allowing only upward transitions and two allowing only downward transitions. At level n , a process in phase 1 or phase 2 can increase to level $n + 1$, transitioning to any phase at rates r_1 and r_2 , respectively. Downward transitions occur from phase 3 or phase 4 to level $n - 1$, again allowing transitions to any phase at rates r_3 and r_4 . The diagonal block $\mathbf{Q}^{[n,n]}$ includes rates r_5 through r_8 , which govern within-level persistence in each phase.

QBD4 has five phases with two allowing only upward transitions and two allowing only downward transitions. We introduce a parameter α that governs the tendency to stay in the same phase upon changing level. At level n , a process in phase 1 can increase to level $n + 1$, remaining in the same phase with rate αr_1 or moving to phase 2 with rate $(1 - \alpha)r_1$. Similarly, a process in phase 2 at level n can increase to level $n + 1$, remaining in phase 2 with rate αr_2 , or moving to phase 1 or phase 3 with rate $(1 - \alpha)r_2/2$ for each transition. Downward transitions occur from phase 4, where the process can move from level n to level $n - 1$ in phase 3, phase 5, or remain in phase 4 with rates $(1 - \alpha)r_4/2$, $(1 - \alpha)r_4/2$, and αr_4 , respectively. Similarly, a process in phase 5 at level n can decrease to level $n - 1$, remaining in phase 5 with rate αr_5 or moving to phase 4 with rate $(1 - \alpha)r_5$. Also, a process in phase 3 at level n can stay in the same level n phase 3 with a rate r_3 , remaining in the same level but moving into phase 2 or phase 4 with rate $(1 - \beta)r_3$ or moving to phase 4 with rate βr_3 . Values of $\beta < 0.5$ give a process with negative drift and values $\beta > 0.5$ give positive drift. For all examples in this paper we take $\alpha = 0.9$, so that changes in level usually do not result in a change in phase.

Across all datasets and QBD models, we assume a uniform distribution of the ancestral (parent) trait value.

4.2 Search for parameters to maximise the likelihood

To numerically optimise the parameters of the QBDs we used both the Nelder-Mead [19] and BFGS [10] methods. These were chosen as they do not require a gradient function (Nelder-Mead is derivative free and BFGS is a quasi-Newton method that uses gradient information to approximate the Hessian). Our

parameters are all nonnegative (they are rates), but to avoid doing constrained optimization, we used the common technique of optimizing the log-transformed parameters.

As numerical optimisation can be prone to getting stuck in local optima, we applied a multi-start optimisation approach in which a different set of initial parameters is used at the start of each iteration of these algorithms. Further, to avoid underflow (i.e. numbers less than machine precision which would affect the correct computation of the likelihood), in place of (8), we apply our factor-scaled likelihood evaluations with

$$\mathbf{f}_M(T^{*(k,B)}(t_N, t)) = \begin{cases} \mathbf{P}_{m(k,B)}(b_k) \times \mathbf{1} & k < \ell_N, \\ M \times (\mathbf{P}_{m(k,B)}(b_k) \times \mathbf{1}) \odot (\mathbf{P}_{m(k+1,B)}(b_{k+1}) \times \mathbf{1}) & k = \ell_B, \\ \mathbf{P}_{m(k+1,N)}(b_k) \times \mathbf{1} & k > \ell_B, \end{cases} \quad (14)$$

for some large M , and then use

$$\mathbf{f}(T^{*(k,B)}(t_1, t)) = \mathbf{f}_M(T^{*(k,B)}(t_1, t))/M^B, \quad (15)$$

or equivalently,

$$\log(\mathbf{f}(T^{*(k,B)}(t_1, t))) = \log(\mathbf{f}_M(T^{*(k,B)}(t_1, t))) - B \times \log(M). \quad (16)$$

5 Numerical Examples: Synthetic Data

We constructed two small synthetic datasets, each consisting of four tips and three internal nodes (Figures 3 and 4), to explore alternative patterns of trait evolution. In the first dataset, two closely related tips sharing a recent common ancestor exhibit low trait values, whereas the two tips branching closer to the root display higher values. In the second dataset, this pattern is reversed, with more basally branching taxa exhibiting lower trait values.

5.1 Synthetic Dataset 1

In our examples in this section, we assume a tree topology with 4 tips and 3 internal nodes as depicted in Figure 3.

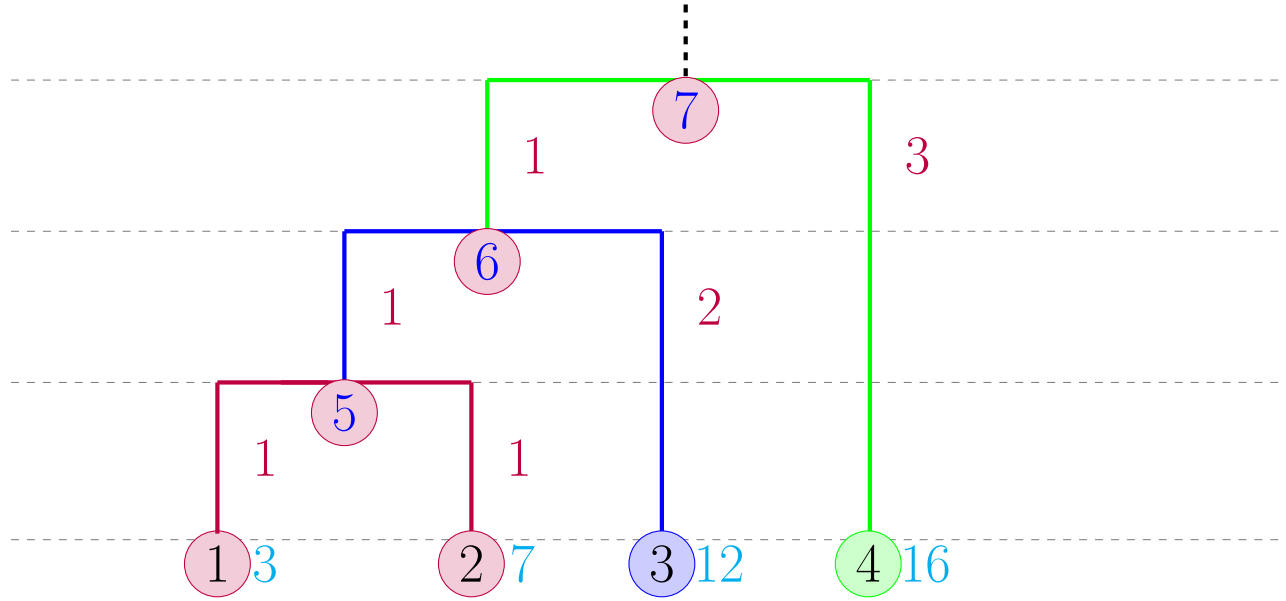


Figure 3: Phylogenetic tree with nodes $1, \dots, 7$, including tips $1, \dots, 4$, internal nodes $5, 6$ and parent node 7 . Branch lengths are indicated along each edge. Observed trait values are indicated to the right of each tip.

5.1.1 QBD3 – Preliminaries: The effect of the mean drift γ

First, to study the effect of the mean drift γ , we consider QBD3 from Table 1 with

$$\mathbf{Q}^{[n,n+1]} = \begin{bmatrix} r_1 & r_1 & r_1 & r_1 & r_1 \\ r_2 & r_2 & r_2 & r_2 & r_2 \\ 0 & 0 & 0 & 0 & 0 \\ 0 & 0 & 0 & 0 & 0 \\ 0 & 0 & 0 & 0 & 0 \end{bmatrix}, \quad \mathbf{Q}^{[n,n-1]} = \begin{bmatrix} 0 & 0 & 0 & 0 & 0 \\ 0 & 0 & 0 & 0 & 0 \\ r_3 & r_3 & r_3 & r_3 & r_3 \\ r_4 & r_4 & r_4 & r_4 & r_4 \\ 0 & 0 & 0 & 0 & 0 \end{bmatrix},$$

$$\mathbf{Q}^{[n,n]} = \begin{bmatrix} -5r_1 & 0 & 0 & 0 & 0 \\ 0 & -5r_2 & 0 & 0 & 0 \\ 0 & 0 & -5r_3 & 0 & 0 \\ 0 & 0 & 0 & -5r_4 & 0 \\ r_5 & r_6 & r_7 & r_8 & -(r_5 + r_6 + r_7 + r_8) \end{bmatrix}, \quad (17)$$

and the range of parameters in Table 2. A more detailed set of results is presented in Figures 9–16 in Appendix A.

r#	r = [$r_1 \dots r_8$]	drift γ	Likelihood	LogLikelihood	AICc
1	[2 1 4 3 2 1 6 5]	-1.0169	6.9049×10^{-22}	-48.7246	84.6492
2	[10 3 5 5 4 6 1 1]	2.2472	2.7730×10^{-15}	-33.5188	54.2376
3	[12 7 8 8 4 6 1 1]	3.2909	1.1775×10^{-12}	-27.4676	42.1352
4	[10 3 8 8 9 10 7 7]	0.7455	4.1574×10^{-13}	-28.5087	44.2174
5	[9 6 7 7 5 7 3 3]	1.6928	7.6748×10^{-13}	-27.8957	42.9914
6	r#1 $\times 10$	-10.1695	3.0103×10^{-10}	-21.9238	31.0476
7	r#2 $\times 10$	22.4719	8.2780×10^{-15}	-32.4252	52.0504
8	r#3 $\times 10$	32.9089	7.8435×10^{-19}	-41.6894	70.5788
9	r#4 $\times 10$	7.4553	4.4464×10^{-9}	-19.2312	25.6624
10	r#5 $\times 10$	16.9279	4.9853×10^{-11}	-23.7219	34.6438

Table 2: The likelihood of the Synthetic Dataset 1 (Figure 3) for the different parameters of QBD3, assuming uniform initial distribution of levels and phases at the root of the tree, and $[a, b] = [3, 20]$.

We first conducted a preliminary analysis using manually selected rate vectors, **r** #1–#10, as provided in Table 2, to illustrate the range of behaviours and insights offered by QBD models exhibiting zero drift, positive drift, or negative drift. The corresponding drift and likelihood results are reported in the respective columns of Table 2 and are further illustrated in Figures 9–16 in Appendix A.1 and A.2. Table 2 shows that the best parameter set **r** #9 has positive drift. One reason why a model with positive drift might be preferred, even though the mean of the trait values observed at the tips is 9.5 which is less than the halfway point between 3 and 20, is that the two longer branches end in higher trait values and must be reached independently, whereas the two smaller trait values can be explained by a shared path from the root (node 7) to their common ancestor (node 5).

In the QBD model with **r** vector #1 in Table 2, which represents a negative mean drift, the stationary distribution of levels (Figure 9) peaks at 0. Similarly, the stationary distribution of traits (Figure 12) becomes concentrated near the trait’s minimum. This pattern reflects the tendency of negative drift to reduce levels (trait values) over time. Furthermore, in a QBD with a negative mean drift, the likelihood of observing tips $i = 1, \dots, 4$ given initial trait x reaches its maximum to the right of the observed tip trait values (Figure 13). This is because the initial trait values would decrease due to negative drift.

In contrast, for QBD models exhibiting positive mean drift (corresponding to **r** vectors #2–#4), increasing the drift strength (γ) progressively shifts the stationary distribution of levels (Figure 9) toward the upper boundary. Similarly, the stationary distribution of trait values (Figure 12) becomes increasingly concentrated near the maximum level, indicating a long-term tendency for the trait to increase. This is expected, as positive drift drives levels upward, causing trait values to approach the upper boundary over time. Furthermore, in QBD models with a positive mean drift, the likelihood of observing tips $i = 1, \dots, 4$ given initial trait x reaches its maximum to the left of the observed tip trait values (Figure 13). This is expected, as positive drift causes the trait values to increase over time from

their initial states.

For the QBD model with negative mean drift, the likelihood of observing the phylogenetic tree given an initial trait value x and phase φ (Figure 15) is higher for phases 3 and 4, which correspond to transitions toward lower levels. Also, the initial trait values x for QBD models with negative drift are higher than those for QBDs with positive mean drift (Figure 13). This is because, under negative drift, higher initial trait values tend to decrease over time, resulting in lower trait values at the tips. In contrast, for QBD models with a positive mean drift, the likelihood of observing the phylogenetic tree given initial trait x and phase φ (Figure 15) is highest for upward-moving phases 1 and 2. For instance, in the QBD model with vector $r\#1$ (negative mean drift), the maximum likelihood occurs in phase $\varphi = 3$ at trait value $x = 13$, illustrating a scenario where traits originate at higher values and gradually drift downward. Conversely, in the QBD model with r vector $\#4$ (positive mean drift), the peak likelihood is found in phase $\varphi = 1$ at trait value $x = 9$, illustrating a scenario where traits originate at lower values and gradually drift upward. Moreover, as the strength of the positive drift increases traits are likely to start from lowest trait value at the top (Figure 16).

5.1.2 QBD0: with 2 phases

Recall the simple QBD with 2 phases in Table 1 such that

$$\mathbf{Q}^{[n,n+1]} = \begin{bmatrix} \lambda/2 & \lambda/2 \\ 0 & 0 \end{bmatrix}, \quad \mathbf{Q}^{[n,n-1]} = \begin{bmatrix} 0 & 0 \\ \mu/2 & \mu/2 \end{bmatrix}, \quad \mathbf{Q}^{[n,n]} = \begin{bmatrix} -\lambda & 0 \\ 0 & -\mu \end{bmatrix} \quad (18)$$

where λ is the rate of moving up in phase 1, and μ is the rate of moving down in phase 2.

We applied QBD0 to the analysis of Synthetic Dataset 1 shown in Figure 3. We set $\lambda = \mu$ to enforce neutral trait evolution without directional bias. The Nelder–Mead optimization produced parameter estimates that maximized the log-likelihood and minimized the $AICc$ (Table 3).

Method	$\lambda = \mu$	Drift γ	Likelihood	LogLikelihood	$AICc$
Manual	10	0	4.8771×10^{-22}	-49.0723	114.1446
Nelder-Mead	576.3080	0	1.2336×10^{-8}	-18.2108	52.4216
BFGS	53925584.9996	0	9.6098×10^{-9}	-18.4605	52.9210

Table 3: The likelihood of the Synthetic Dataset 1 (Figure 3) for the different parameters of QBD0, assuming uniform initial distribution of levels and phases at the root of the tree, and $[a, b] = [3, 20]$.

5.1.3 QBD1: with 3 phases

Next, we consider the QBD with 3 phases in Table 1 such that

$$\mathbf{Q}^{[n,n+1]} = \begin{bmatrix} 0 & \lambda_1 & \lambda_2 \\ 0 & 0 & 0 \\ \lambda_3 & 0 & 0 \end{bmatrix}, \quad \mathbf{Q}^{[n,n-1]} = \begin{bmatrix} 0 & 0 & 0 \\ \mu/3 & \mu/3 & \mu/3 \\ 0 & 0 & 0 \end{bmatrix}, \quad \mathbf{Q}^{[n,n]} = \begin{bmatrix} -(\lambda_1 + \lambda_2) & 0 & 0 \\ 0 & -\mu & 0 \\ 0 & 0 & -\lambda_3 \end{bmatrix} \quad (19)$$

and apply it to the analysis of dataset shown in Figure 3.

Both the Nelder–Mead and BFGS optimisation methods converged on solutions that exhibit positive drift (Table 4). The BFGS algorithm yielded optimal maximum-likelihood estimates with positive drift ($\gamma = 13.3295$), achieving the highest log-likelihood and the minimum AICc scores (Table 4).

Method	$[\lambda_1, \lambda_2, \lambda_3]$ and μ	Drift γ	Likelihood	LogLikelihood	AICc
Manual	[10, 0.1, 0.1] and 10	0.0037	1.2049×10^{-47}	-108.0351	184.0702
Nelder-Mead	[282.5302, 418439145.5456, 10] and 10	20.0000	3.3185×10^{-21}	-47.1548	62.3096
BFGS	[1.6023, 14.5773, 89.2153] and 2.3682	13.3295	3.2841×10^{-10}	-21.8368	11.6736

Table 4: The likelihood of the Synthetic Dataset 1 (Figure 3) for the different parameters of the QBD1, assuming uniform initial distribution of levels and phases at the root of the tree, and $[a, b] = [3, 20]$.

5.1.4 QBD2: with 4 phases

We then applied the QBD model with 4 phases in Table 1 such that

$$\begin{aligned}
 \mathbf{Q}^{[n,n+1]} &= \begin{bmatrix} 0 & \lambda_1 & \lambda_2 & \lambda_3 \\ 0 & 0 & 0 & 0 \\ \lambda_4 & \lambda_5 & 0 & 0 \\ 0 & 0 & 0 & 0 \end{bmatrix}, & \mathbf{Q}^{[n,n-1]} &= \begin{bmatrix} 0 & 0 & 0 & 0 \\ \mu_1 & 0 & \mu_2 & \mu_3 \\ 0 & 0 & 0 & 0 \\ \mu_4 & \mu_5 & 0 & 0 \end{bmatrix}, \\
 \mathbf{Q}^{[n,n]} &= \begin{bmatrix} -(\lambda_1 + \lambda_2 + \lambda_3) & 0 & 0 & 0 \\ 0 & -(\mu_1 + \mu_2 + \mu_3) & 0 & 0 \\ 0 & 0 & -(\lambda_4 + \lambda_5) & 0 \\ 0 & 0 & 0 & -(\mu_4 + \mu_5) \end{bmatrix}. \tag{20}
 \end{aligned}$$

to the analysis of dataset shown in Figure 3.

The Nelder–Mead optimisation method converged on parameter estimates with a negative drift, while the BFGS algorithm produced estimates with very small positive drift. None of the parameter estimates found for this model performed as well in terms of AICc as QBD1 suggesting that numerical optimization is struggling to fit the 10 parameter model.

Method	$[\lambda_1, \dots, \lambda_5]$	$[\mu_1, \dots, \mu_5]$	Drift γ	Likelihood	Log-Likelihood	AICc
Manual	[10, 0.1, 0.1, 1, 1]	[10, 0.1, 0.1, 1, 1]	0	1.478×10^{-101}	-232.1701	452.9116
Nelder-Mead	[42.6160, 0.0003, 0.0000, 0.0000, 1.0098]	[1.5126, 0.0000, 310726, 0.0001, 1.0248]	-2.0497	4.624×10^{-42}	-95.1166	178.8046
BFGS	[2.1530, 4.9817, 6.0689, 2.2324, 1.5064]	[0.0990, 0.0833, 0.0593, 0.0451, 0.0763]	1.590×10^{-2}	1.434×10^{-68}	-156.2150	301.0014

Table 5: The likelihood of the Synthetic Dataset 1 (Figure 3) for the different parameters of QBD2, assuming uniform initial distribution of levels and phases at the root of the tree, and $[a, b] = [3, 20]$.

5.1.5 Comparison of QBD Model Fits for Synthetic Dataset 1 (Figure 3)

Of the three models we evaluated, the QBD1 model, fitted using BFGS optimisation, yielded maximum-likelihood estimates with a positive drift and provided the best fit to Synthetic Dataset 1 (minimum $AICc = 11.6736$; Table 4). This result indicates that the observed trait values at the tips are best explained by a process that tends to increase toward the upper boundary of the trait range ($b = 20$).

5.2 Synthetic Dataset 2

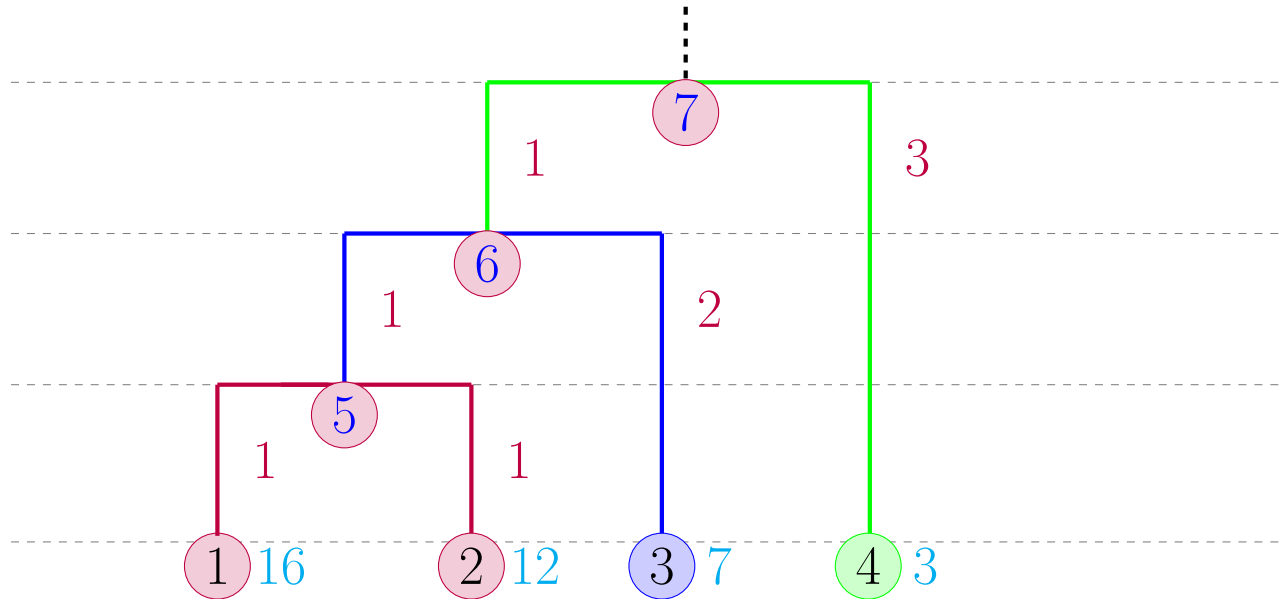


Figure 4: Phylogenetic tree with nodes $1, \dots, 7$, including tips $1, \dots, 4$, internal nodes $5, 6$ and parent node 7 . Branch lengths are indicated along each edge. Observed trait values are indicated to the right of each tip.

5.2.1 QBD3 – Preliminaries: The effect of the mean drift γ

First, to study the effect of the mean drift γ , we consider a QBD with the block matrices in (17) for a selected range of parameters, the output is presented in Table 6.

r#	r = [$r_1 \dots r_8$]	Drift γ	Likelihood	LogLikelihood	AICc
1	[2 1 4 3 2 1 6 5]	-1.0169	6.1049×10^{-23}	-51.1504	89.5008
2	[10 3 5 5 4 6 1 1]	2.2472	1.5023×10^{-17}	-38.7370	64.6740
3	[12 7 8 8 4 6 1 1]	3.2909	7.8723×10^{-15}	-32.4754	52.1508
4	[10 3 8 8 9 10 7 7]	0.7455	5.4629×10^{-14}	-30.5382	48.2764
5	[9 6 7 7 5 7 3 3]	1.6928	5.6480×10^{-14}	-30.5049	48.2098
6	r#1 $\times 10$	-10.1695	2.0926×10^{-8}	-17.6823	22.5646
7	r#2 $\times 10$	22.4719	6.6542×10^{-17}	-37.2487	61.6974
8	r#3 $\times 10$	32.9089	1.0621×10^{-21}	-48.2940	83.7880
9	r#4 $\times 10$	7.4553	7.6177×10^{-10}	-20.9954	29.1908
10	r#5 $\times 10$	16.9279	2.5789×10^{-12}	-26.6837	40.5674

Table 6: The likelihood of the Synthetic Dataset 2 (Figure 4) for the different parameters of QBD3, assuming uniform initial distribution of levels and phases at the root of the tree, and $[a, b] = [3, 20]$.

To investigate the extent to which the structure of the tree affects the preference for different levels of drift we used the same set of rate parameters explored in Table 2 but applied to Synthetic Dataset 2 where the order of the traits is reversed compared to Synthetic Dataset 1. The corresponding drift and the likelihood results for these rates for the QBD4 model are provided in Table 6 and are further illustrated in Appendix A.3 In this case we found that the best performing parameter set, **r#6**, has negative drift. This difference to what we saw for Synthetic Dataset 1 is interesting, we note that in synthetic dataset 2 the two lowest trait values have to be reached independently, whereas the two larger trait values can be reached by a shared path. Combined with the results from synthetic dataset 1, this indicates that the structure of the tree, as well as the observed trait values, influences the preferred level of drift.

Consistent with Synthetic Dataset 1 (Figure 3), in Synthetic Dataset 2 (Figure 4), the likelihood of observing tips $i = 1, \dots, 4$ given the initial trait x peaks to the right of the observed traits under negative drift and to the left under positive drift.

For Synthetic Dataset 2 (Figure 4), the likelihood of observing the tree under a QBD model with negative drift was highest when starting in phase $\varphi = 4$, with levels ranging from 40 to 100 (Figure 18). In contrast, in a QBD model with small positive drift, the most likely starting phase was phase $\varphi = 1$, with initial levels ranging from 10 to 50 (Figure 18). Phase $\varphi = 3$ corresponds to transitions toward lower levels, whereas phase $\varphi = 1$ corresponds to transitions toward upper levels. Furthermore, initial trait values x for QBD models with a negative drift were higher than those for QBD models with a positive mean drift (Figure 20).

5.2.2 QBD0: with 2 phases

We then applied a simple two-phase QBD model, summarised in Table 1 and defined by the generator in Equation (18), to Synthetic Dataset 2 (Figure 4). The best set of parameters was found using Nelder–Mead optimisation (Table 7).

Method	$\lambda = \mu$	Drift γ	Likelihood	LogLikelihood	AICc
Manual	10	0	3.5576×10^{-22}	-49.3878	114.7756
Nelder-Mead	1945.2130	0	9.6234×10^{-9}	-18.4591	52.9182
BFGS	300	0	6.6114×10^{-9}	-18.8345	53.6690

Table 7: The likelihood of the Synthetic Dataset 2 (Figure 4) for the different parameters of QBD0, assuming uniform initial distribution of levels and phases at the root of the tree, and $[a, b] = [3, 20]$.

5.2.3 QBD1: with 3 phases

We also applied the QBD1 model, summarised in Table 1 and defined by the generator in equation (19), to Synthetic Dataset 2 (Figure 4). The best-fitting parameter estimates were obtained using BFGS optimisation; the resulting parameter estimates yielded zero drift (Table 8). Based on our arguments above, here we expected the model to prefer negative drift values. However, numerical exploration (a million random choices of the parameters) suggests that the structure of this model makes it impossible to achieve negative drift. This is presumably because the level can only go downwards when in phase 2, and when it does it will change to phase 1 or 3 with $2/3$ probability and from these phases it can only go up. Whereas when it goes up a level it is possible to remain in phase 1 or 3 and then go up again.

Method	$[\lambda_1, \lambda_2, \lambda_3]$ and μ	Drift γ	Likelihood	LogLikelihood	AICc
Manual	[10, 0.1, 0.1] and 10	0.0037	8.9698×10^{-69}	-156.6845	281.3690
Nelder-Mead	[137641922.0985, 0.0479, 1158.7438] and 21155242.3867	1.6127×10^{-06}	1.0008×10^{-08}	-18.4199	4.8398
BFGS	[366976194.7948, 0.0362, 910.2207] and 50293301.1721	3.5913×10^{-7}	1.0012×10^{-08}	-18.4195	4.8390

Table 8: The likelihood of the Synthetic Dataset 2 (Figure 4) for the different parameters of QBD1, assuming uniform initial distribution of levels and phases at the root of the tree, and $[a, b] = [3, 20]$.

5.2.4 QBD2: with 4 phases

We also applied QBD2 model with 4 phases, summarised in Table 1 and defined in equation 20, to the dataset shown in Figure 4. Optimisation using the BFGS algorithm yielded parameter estimates with a small positive drift whereas a parameter estimation using Nelder-Mead yielded a parameter estimates with small negative drift. However, similar to Synthetic Dataset 1 (Figure 3), numerical optimisation appears to struggle to fit the 10-parameter model as evidenced by the large AICc values compared to other models (Table 9).

Method	$[\lambda_1, \dots, \lambda_5]$	$[\mu_1, \dots, \mu_5]$	Drift γ	Likelihood	Log-Likelihood	AICc
Manual	[10, 0.1, 0.1, 1, 1]	[10, 0.1, 0.1, 1, 1]	≈ 0	6.0005×10^{-102}	-233.0718	491.9331
Nelder-Mead	[0.2134, 0.8380, 4.4182, 0.3612, 4.9838]	[0.0027, 0.0074, 0.0043, 0.0036, 0.0072]	-0.0048	1.7562×10^{-103}	-236.6031	498.9957
BFGS	[2.1530, 4.9817, 6.0689, 2.2324, 1.5064]	[0.0990, 0.0833, 0.0593, 0.0451, 0.0763]	0.0159	1.2312×10^{-46}	-105.7109	237.2113

Table 9: The likelihood of the Synthetic Dataset 2 (Figure 4) for the different parameters of QBD2, assuming uniform initial distribution of levels and phases at the root of the tree, and $[a, b] = [3, 20]$.

5.2.5 Comparison of QBD Model Fits for Synthetic Dataset 2 (Figure 4)

The zero-drift QBD1 model provided the best fit to Synthetic Dataset 2 (Figure 4), yielding the minimum $AICc = 4.839$. However, as numerical methods did not appear to do a good job of exploring models that allow negative drift we don't read too much into this.

6 Numerical Examples: Empirical Data

In this section, we analyse a phylogenetic tree representing the evolutionary relationships among 49 mammal species, as depicted in Figures 5 and 7. Trait measurements, home-range area (km^2) and body mass (kg), are observed at the terminal tips. The datasets originate from Garland et al. [11] and are available through the phytools R package [24]. For the analysis we applied a selection of different parameter values for QBD3 (5 phases) to explore different values of mean drift, we also compare to QBD0 (2 phases, no drift) and a selection of parameters for QBD4 (5 phases).

6.1 Empirical Dataset 1: Body mass (kg)

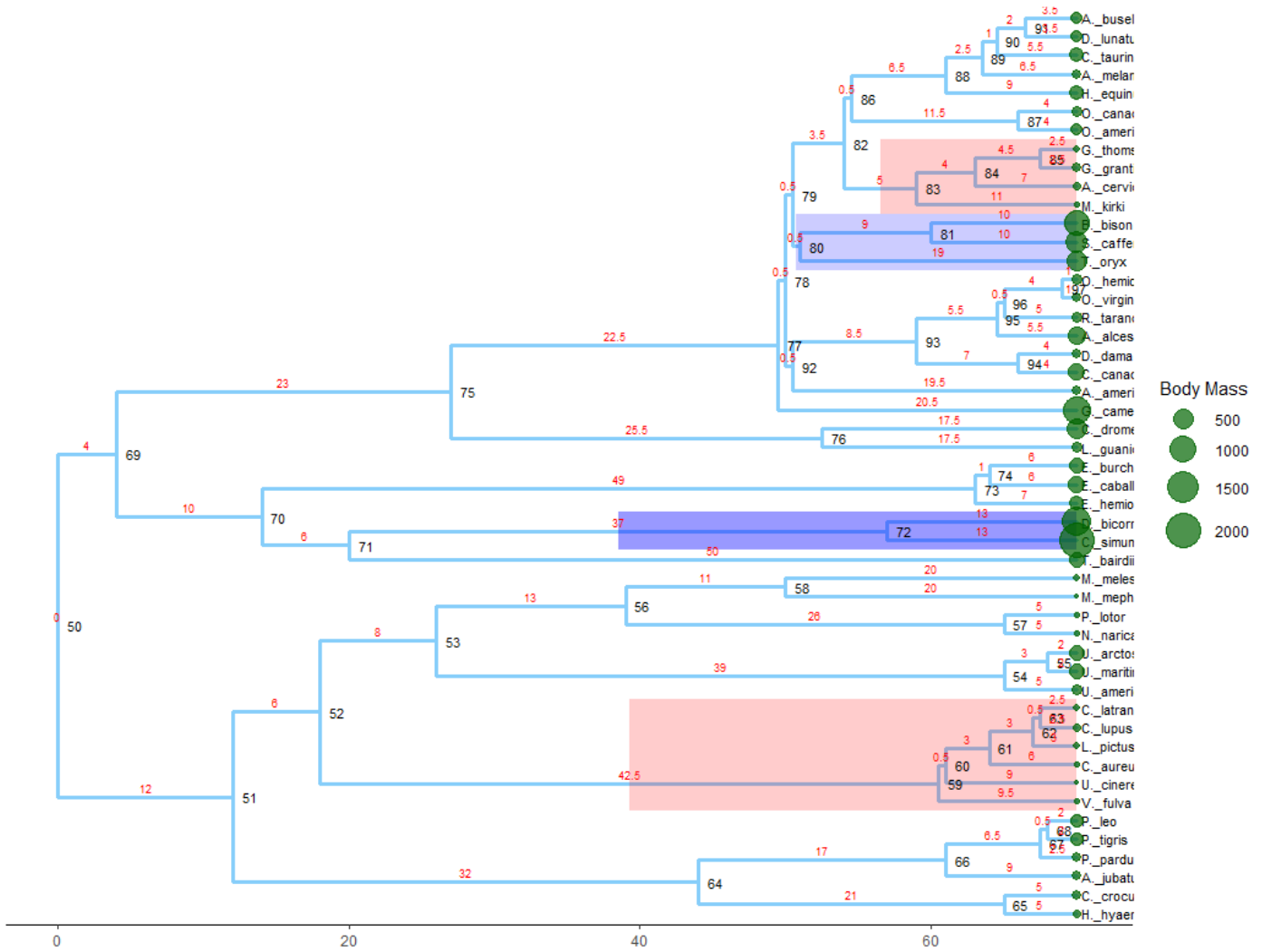


Figure 5: A phylogenetic tree of 49 mammal species, with branch lengths shown on the edges in red, nodes in black, and body mass values (kg) displayed at the tips using circles of varying size. Trait values range from $a = 2.5$ to $b = 2000$. Circle sizes are proportional to body mass, with smaller circles representing smaller species and larger circles representing larger species.

6.1.1 Histogram of observed body mass

The histogram in Figure 6 reveals a right-skewed distribution of body mass, showing that the majority of species are smaller-bodied. Observed body mass values ranges from 2.5kg to 2000kg, with approximately 75% of species falling below 250kg (Figure 6). We further aim to use the QBD model to underscore whether the observed trait values at the tips were driven by negative drift or zero drift, implying they were already small at their ancestral states, or whether they were initially very small and increased due to positive drift.

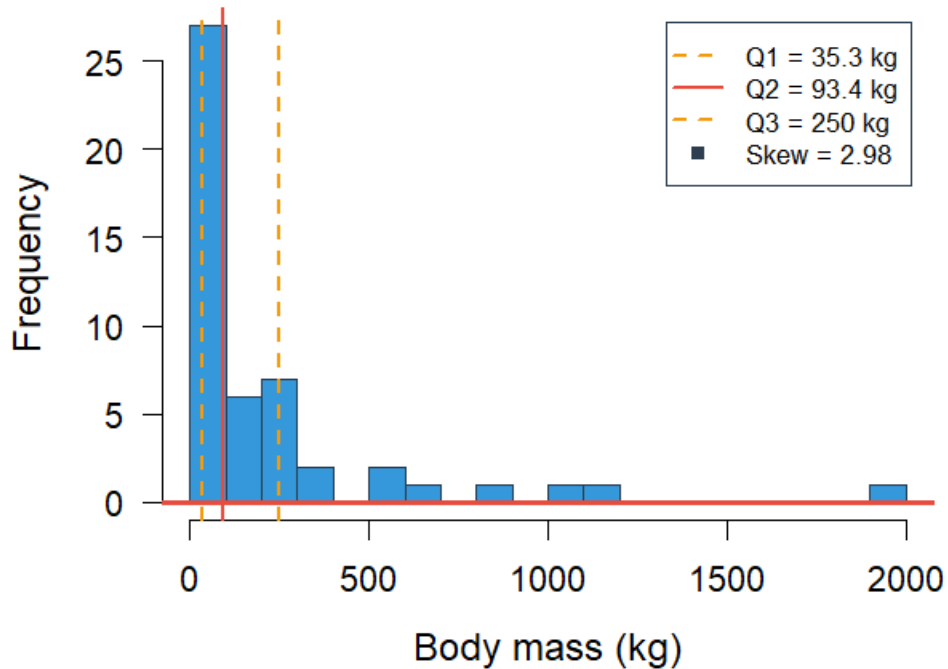


Figure 6: Histogram of body mass (kg) showing positive skew with most values concentrated at the lower ranges.

6.1.2 QBD3 with 5 phases

We performed the analysis for the \mathbf{r} vectors #1 – #5 as shown in Table 10 (\mathbf{r} values and drift are analogous to Table 2). The output of this analysis is also presented in Figures 21-24 in Appendix B.

$\mathbf{r}\#$	$\mathbf{r} = [r_1 \dots r_8]$	drift γ	Likelihood	LogLikelihood
1	[2 1 4 3 2 1 6 5]	-1.0169	1.3951×10^{-70}	-160.8480
2	[10 3 5 5 4 6 1 1]	2.2472	2.8247×10^{-180}	-413.4269
3	[12 7 8 8 4 6 1 1]	3.2909	3.0596×10^{-227}	-521.5685
4	[10 3 8 8 9 10 7 7]	0.7455	2.0960×10^{-94}	-215.7030
5	[9 6 7 7 5 7 3 3]	1.6928	7.2798×10^{-128}	-292.7458

Table 10: The likelihood of the Empirical Dataset 1 (Figure 5) for the different parameters of QBD3, assuming uniform initial distribution of levels and phases at the root, and $a = 2.5$, $b = 2000$.

6.1.3 QBD0: with 2 phases

$\lambda = \mu$	drift γ	Likelihood	LogLikelihood
10	0	7.8129×10^{-75}	-170.6381

Table 11: The likelihood of the Empirical Dataset 1 (Figure 5) for the QBD0 model, assuming uniform initial distribution of levels and phases at the root of the tree, and $a = 2.5$, $b = 2000$.

6.1.4 QBD4 with 5 phases

We then applied the QBD4 model with 5 phases, summarised in Table 1, with $\alpha = 0.9$, for the various values of parameters β , with

$$\begin{aligned}
 \mathbf{Q}^{[n,n+1]} &= \begin{bmatrix} \alpha r_1 & (1-\alpha)r_1 & 0 & 0 & 0 \\ \frac{(1-\alpha)r_2}{2} & \alpha r_2 & \frac{(1-\alpha)r_2}{2} & 0 & 0 \\ 0 & 0 & 0 & 0 & 0 \\ 0 & 0 & 0 & 0 & 0 \\ 0 & 0 & 0 & 0 & 0 \end{bmatrix}, \\
 \mathbf{Q}^{[n,n-1]} &= \begin{bmatrix} 0 & 0 & 0 & 0 & 0 \\ 0 & 0 & 0 & 0 & 0 \\ 0 & 0 & 0 & 0 & 0 \\ 0 & 0 & \frac{(1-\alpha)r_4}{2} & \alpha r_4 & \frac{(1-\alpha)r_4}{2} \\ 0 & 0 & 0 & (1-\alpha)r_5 & \alpha r_5 \end{bmatrix}, \\
 \mathbf{Q}^{[n,n]} &= \begin{bmatrix} -r_1 & 0 & 0 & 0 & 0 \\ 0 & -r_2 & 0 & 0 & 0 \\ 0 & (1-\beta)r_3 & -r_3 & \beta r_3 & 0 \\ 0 & 0 & 0 & -r_4 & 0 \\ 0 & 0 & 0 & 0 & -r_5 \end{bmatrix}. \tag{21}
 \end{aligned}$$

The output is presented in Table 12.

α	β	$[r_1 \dots r_5]$	drift γ	Likelihood	LogLikelihood
0.9	0.70	$[2, 1, \frac{1}{2}, 1, 2]$	-0.4444	1.3296×10^{-66}	-151.6857
0.9	0.50	$[1, 1, 1, 1, 1]$	0	1.2656×10^{-65}	-149.4325
0.9	0.70	$[1, 1, 1, 1, 1]$	-0.3871	1.7394×10^{-65}	-149.1145
0.9	0.30	$[1, 1, 1, 1, 1]$	0.3871	1.2126×10^{-65}	-151.7779

Table 12: The likelihood of the Empirical Dataset 1 (Figure 5) for the QBD4 model, assuming uniform initial distribution of levels and phases at the root of the tree, and $a = 2.5$, $b = 2000$.

6.2 Empirical Dataset 2: Home range area (km^2)

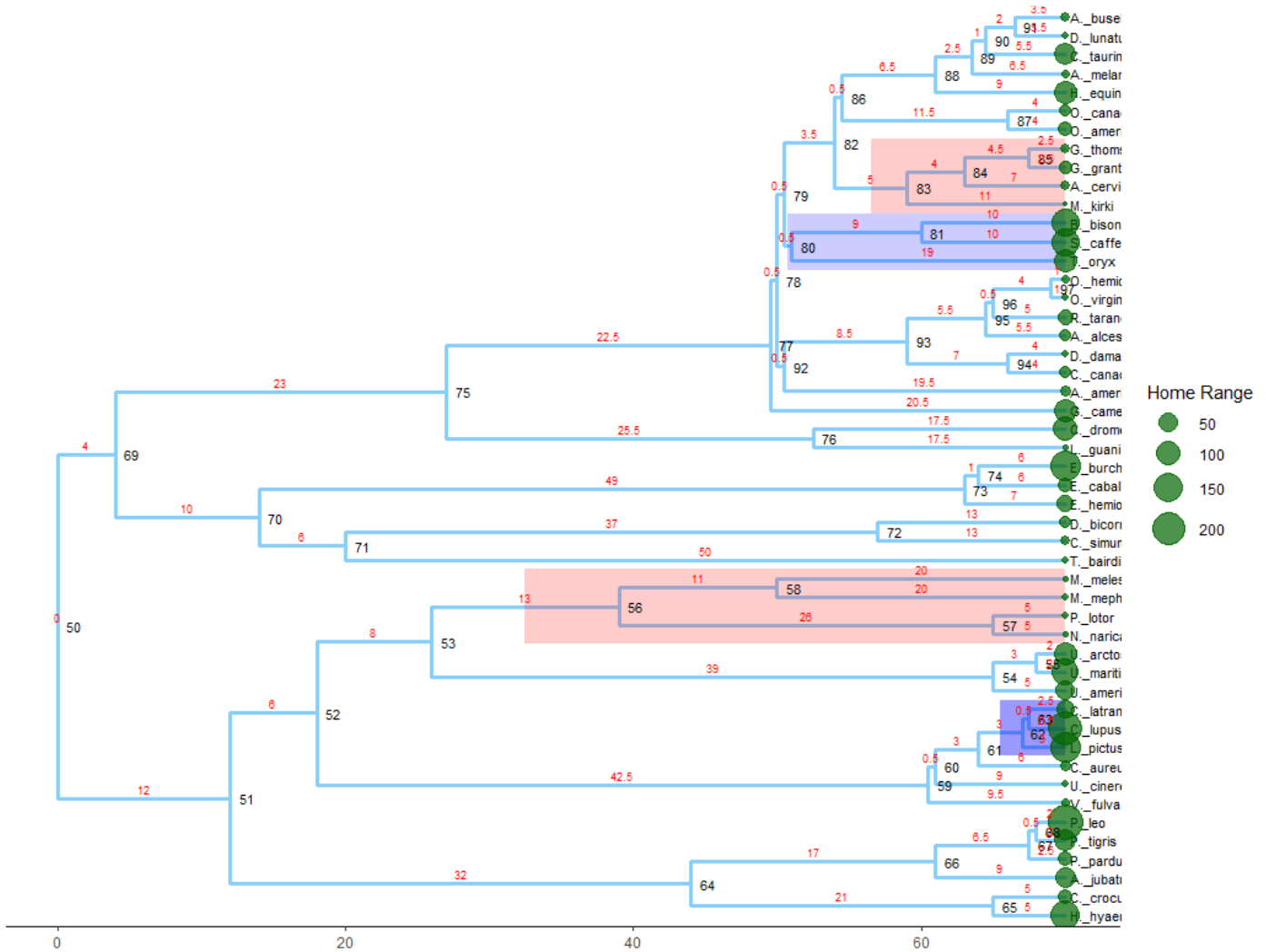


Figure 7: Phylogenetic tree of 49 mammal species showing home range area values (km^2) at the tips. Trait values range from $a = 0.043$ to $b = 236$. Circle sizes are proportional to home range area, with smaller circles representing species occupying smaller territories and larger circles representing those with more extensive ranges.

6.2.1 Histogram of observed home range area

Similar to the histogram of body mass (kg), the histogram of home range area (km^2) in Figure 8 reveals a right-skewed distribution, indicating majority of the species occupy relatively small ranges. Observed home range areas span from 0.043 km^2 to 236 km^2 , with approximately 75% of species fall below 80 km^2 .

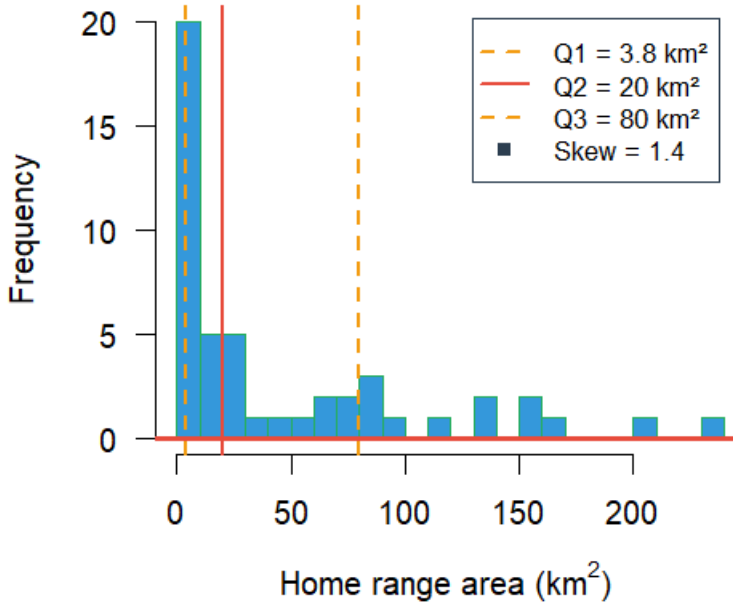


Figure 8: Histogram of home range area (km^2) showing positive skew with most values concentrated at the lower ranges.

6.2.2 QBD3 with 5 phases

We performed the analysis for the \mathbf{r} vectors #1 – #5 as shown in Table 13 (\mathbf{r} values and drift are analogous to Table 2). The output of this analysis is also presented in Figures 25-28 in Appendix C.

$\mathbf{r}\#$	$\mathbf{r} = [r_1 \dots r_8]$	drift γ	Likelihood	LogLikelihood
1	[2 1 4 3 2 1 6 5]	-1.0169	4.6623×10^{-126}	-288.5862
2	[10 3 5 5 4 6 1 1]	2.2472	2.1913×10^{-199}	-457.4299
3	[12 7 8 8 4 6 1 1]	3.2909	2.3053×10^{-236}	-542.5748
4	[10 3 8 8 9 10 7 7]	0.7455	1.6930×10^{-114}	-261.9682
5	[9 6 7 7 5 7 3 3]	1.6928	9.8633×10^{-143}	-326.9809

Table 13: The likelihood of the Empirical Dataset 2 (Figure 5) for the different parameters of QBD3, assuming uniform initial distribution of levels and phases at the root of the tree, and $a = 0.043$, $b = 236$.

6.2.3 QBD0: with 2 phases

$\lambda = \mu$	drift γ	Likelihood	LogLikelihood
10	0	2.6742×10^{-125}	-286.8395

Table 14: The likelihood of the Empirical Dataset 2 (Figure 7) under the QBD0 model, assuming uniform initial distribution of levels and phases at the root of the tree, and $a = 0.043$, $b = 236$.

6.2.4 QBD4 with 5 phases

We then applied the QBD4 model with 5 phases, summarised in Table 1 and generator in (21), with $\alpha = 0.9$, for the various values of parameters β . The output is presented in Table 15.

α	β	$[r_1 \dots r_5]$	drift γ	Likelihood	LogLikelihood
0.9	0.60	$[4, 2, \frac{1}{2}, 1, 2]$	-0.2727	2.3775×10^{-135}	-309.9829
0.9	0.50	$[1, 1, 1, 1, 1]$	0	1.3012×10^{-226}	-520.1209
0.9	0.70	$[1, 1, 1, 1, 1]$	-0.3871	1.5683×10^{-226}	-519.9343
0.9	0.30	$[1, 1, 1, 1, 1]$	0.3871	2.3095×10^{-228}	-524.1524

Table 15: The likelihood of the Empirical Dataset 2 (Figure 7) for the QBD4 model, assuming uniform initial distribution of levels and phases at the root of the tree, and $a = 2.5$, $b = 2000$.

6.3 Comments on the Empirical Datasets 1 and 2

For the two empirical datasets we tested a range of different parameter sets for models QBD3, QBD0 and QBD4. For QBD3 and QBD4 we picked some parameters that give negative drift and some that give positive drift. Recall that compared to QBD3, the $\alpha = 0.9$ parameter in QBD4 enforces that the phases change infrequently compared to the level.

For the body mass dataset with QBD3 the rank of the log likelihoods corresponded to the drift, with the parameters producing negative drift ($\mathbf{r} \#1$) preferred. For the body mass dataset with QBD4 the best parameter set also had negative drift but we note that the parameter set with zero drift and the parameter set with positive drift had a better likelihood than any version of QBD3. QBD0 with no drift did better than the positive drift variants of QBD3 but worse than all variants of QBD4.

For the home range data the rank of the log likelihoods corresponded with increasing absolute value of the drift with the best parameter set having the smallest drift. Most of the QBD3 parameter sets scored better than most of the QBD4 parameter sets. QBD0 performed better than all but one of the QBD3 parameter sets. The best fitting parameter set overall was a QBD3 option with positive drift.

7 Conclusions

We considered a quasi-birth-and-death (QBD) process that undergoes binary branching at certain times to model the evolution of a continuous trait through discretisation. We developed an efficient recursive algorithm for computing the likelihood of observing a phylogenetic tree under a duplicating quasi-birth-and-death (QBD) process. We examined a range of QBD models to capture the evolution of trait dynamics, with parameters estimated via a multi-start optimisation strategy and factor-scaled likelihood evaluations to ensure numerical stability and mitigate underflow. We applied various QBD models to synthetic datasets to illustrate the framework’s general-purpose capability to illustrate a range of behaviours. We also applied biologically motivated QBD structures to two empirical datasets to assess the evidence for positive versus negative drift in these traits. We compared the performance of different QBD structures for each dataset using AICc. Overall, this methodology establishes a foundation for future extensions to other branching stochastic systems and broader applications in queueing and matrix-analytic contexts. Future work may focus on the applications of stochastic fluid models to directly model the evolution of continuous traits without discretisation. While all the examples we explored in this paper used level-independent QBDs, we could also explore level-dependent QBDs to model stabilizing selection for comparative phylogenetic data. For some comparative studies it is of interest to study how different traits coordinate with each other, in this context it would be very interesting to apply recent results by Aksamit et al. [2] who show that a random walk on a quadrant can be analysed as a one-dimensional QBD given an appropriate mapping of the state space.

8 Statements and declarations

Data availability

The authors declare that the data supporting the findings of this study are available within the paper.

Authorship contribution statement

This paper contributes to a chapter in the PhD project by Habtu Kiros Nigus [21]. The following are the contributions of the authors, Habtu Kiros Nigus (HKN), Barbara R. Holland (BRH), Małgorzata M. O’Reilly (MMO).

- Sections 2, 5 and 6, Problem formulation and methodology development: HKN, BRH, and MMO;
- Sections 3, Derivation of the theoretical expressions and algorithms: MMO;
- Sections 5 and 6, Coding: HKN, MMO;
- Sections 5 and 6, Data analysis: HKN;
- Sections 4, 5 and 6, Numerical analysis: HKN;
- Conceptualisation, Biological background: HKN, BRH;

- Conceptualisation, Mathematical background: HKN, BRH, MMO;
- Write-up and edits: HKN, BRH, MMO.

References

- [1] A. Aksamit, M. M. O'Reilly, and Z. Palmowski. Sensitivities of some performance measures of quasi-birth-and-death processes. *Stochastic Models*, 2024.
- [2] A. Aksamit, M. M. O'Reilly, and Z. Palmowski. Random walk on a quadrant: mapping to a one-dimensional level-dependent quasi-birth-and-death process. *Stochastic Models*, 2025.
- [3] N. G. Bean, P. K. Pollett, and P. G. Taylor. Quasistationary distributions for level-dependent quasi-birth-and-death processes. *Communications in Statistics. Part C: Stochastic Models*, 16(5):511–541, 2000.
- [4] J. M. Beaulieu, D.-C. Jhwueng, C. Boettiger, and B. C. O'Meara. Modeling stabilizing selection: expanding the Ornstein–Uhlenbeck model of adaptive evolution. *Evolution*, 66(8):2369–2383, 2012.
- [5] L. Bright and P. G. Taylor. Calculating the equilibrium distribution in level dependent quasi-birth-and-death processes. *Communications in Statistics. Stochastic Models*, 11(3):497–525, 1995.
- [6] M. A. Butler and A. A. King. Phylogenetic comparative analysis: a modeling approach for adaptive evolution. *The american naturalist*, 164(6):683–695, 2004.
- [7] P. Den Iseger. Numerical transform inversion using gaussian quadrature. *Probability in the Engineering and Informational Sciences*, 20(1):1–44, 2006.
- [8] J. Felsenstein. Evolutionary trees from dna sequences: a maximum likelihood approach. *Journal of molecular evolution*, 17:368–376, 1981.
- [9] J. Felsenstein. Phylogenies and the comparative method. *The American Naturalist*, 125(1):1–15, 1985.
- [10] R. Fletcher. *Practical methods of optimization*. John Wiley & Sons, 2000.
- [11] J. Garland, Theodore, P. H. Harvey, and A. R. Ives. Procedures for the Analysis of Comparative Data Using Phylogenetically Independent Contrasts. *Systematic Biology*, 41(1):18–32, 03 1992.
- [12] T. F. Hansen. Stabilizing selection and the comparative analysis of adaptation. *Evolution*, 51(5):1341–1351, 1997.
- [13] Q.-M. He. *Fundamentals of matrix-analytic methods*, volume 365. Springer, 2014.
- [14] L. S. T. Ho and C. Ané. Intrinsic inference difficulties for trait evolution with Ornstein-Uhlenbeck models. *Methods in Ecology and Evolution*, 5(11):1133–1146, 2014.

- [15] G. Horváth, I. Horváth, S. A.-D. Almousa, and M. Telek. Numerical inverse Laplace transformation using concentrated matrix exponential distributions. *Performance Evaluation*, 137:102067, 2020.
- [16] T. Ingram and D. L. Mahler. SURFACE: detecting convergent evolution from comparative data by fitting Ornstein-Uhlenbeck models with stepwise AIC. *Methods in ecology and evolution*, 4(5):416–425, 2013.
- [17] J. Joyner and B. Fralix. A new look at Markov processes of G/M/1-type. *Stochastic Models*, 32(2):253–274, 2016.
- [18] G. Latouche and V. Ramaswami. *Introduction to matrix analytic methods in stochastic modeling*. SIAM, 1999.
- [19] J. A. Nelder and R. Mead. A simplex method for function minimization. *The computer journal*, 7(4):308–313, 1965.
- [20] M. F. Neuts. *Matrix-geometric solutions in stochastic models: an algorithmic approach*, volume 2 of *Johns Hopkins Series in the Mathematical Sciences*. Johns Hopkins University Press, 1981.
- [21] H. K. Nigus. *Stochastic Models for the Conservation of Endangered Species*. PhD thesis, The University of Tasmania, Under preparation.
- [22] T. Phung-Duc, H. Masuyama, S. Kasahara, and Y. Takahashi. A simple algorithm for the rate matrices of level-dependent QBD processes. In *5th International Conference on Queueing Theory and Network Applications, QTNA 2010 - Proceedings*, pages 46–52, 2010.
- [23] V. Ramaswami. Matrix Analytic Methods: A Tutorial Overview with Some Extensions and New Results. In *Matrix-Analytic Methods in Stochastic Models (Flint, MI)*, volume 183 of *Lecture Notes in Pure and Appl. Math.*, pages 261–296. Dekker, New York, 1997.
- [24] L. J. Revell. phytools: an R package for phylogenetic comparative biology (and other things). *Methods in Ecology and Evolution*, (2):217–223, 2012.
- [25] A. C. Soewongsono, J. Diao, T. Stark, A. E. Wilson, D. A. Liberles, B. R. Holland, and M. M. O’Reilly. Matrix-analytic methods for the evolution of species trees, gene trees, and their reconciliation. *Methodology and Computing in Applied Probability*, 27(1):1–47, 2025.

A The effect of the mean drift

To illustrate the effect of the mean drift on the likelihood of observing a given tree, we consider the QBD3 model in Section 4 with five phases, and evaluate the likelihood of the two synthetic datasets for a range of the QBD parameters. First, the stationary distribution of the QBD for the \mathbf{r} vectors #1 – #4 in Table 2 (analogous to Table 6), is presented in Appendix A.1. Next, the output for Synthetic Dataset 1 (Figure 3) and Synthetic Dataset 2 (Figure 4) is presented in Section A.2 and Section A.3, respectively.

We present a series of graphs illustrating the potential behaviours of the QBD3 model, emphasising the effect of mean drift and highlighting key insights obtained from Synthetic Datasets 1 and 2. For this preliminary exploration, we selected parameter vectors designed to induce both negative and positive drift and fitted QBD models with these rates to each dataset.

Figures 9 to 12 in Appendix A.1 depict the stationary distributions of the levels in the QBD3 model, showing the long-term behaviour of the process, whether it tends to converge towards the upper or lower boundary of the levels under positive or negative drift. We also include the stationary distributions of the phases, the states (joint level–phase combinations), and the traits (back-transformed from discretised levels) to illustrate how drift influences overall model dynamics. The stationary distributions over states (n, φ) indicate the long-run probability of occupying each level–phase combination, revealing both the tendency towards lower or higher levels and the corresponding environmental phase most often associated with them.

Figures 13–16 in Appendix A.2 illustrate the behaviours described below for Synthetic Dataset 1 (Figure 3) when analysed under the QBD3 model. Similarly, Figures 17–20 in Appendix A.3 show the corresponding behaviours for Synthetic Dataset 2 (Figure 4) under the same QBD3 model.

Figure 13 (Appendix A.2) and Figure 17 (Appendix A.3) depicts the likelihood of observing each tip $(i = 1, \dots, 4)$ given the initial trait value x at the start of the corresponding branch, illustrating the direction in which the likelihood peaks relative to the observed tip values, that is, whether it shifts to the right or left depending on the QBD process drift condition.

Figures 14–15 (Appendix A.2) and Figures 18–19 (Appendix A.3) illustrate the likelihood of observing the entire phylogenetic tree, conditional on the level n (trait x) and phase φ , highlighting the most probable level–phase (trait–phase) combinations, revealing both the likely initial levels (traits) and their associated environmental phases.

Finally, in Figure 16 (Appendix A.2) and Figure 20 (Appendix A.3) we present the likelihood of observing the phylogenetic tree given the starting trait x , under both positive and negative drift conditions, illustrating whether the process is more likely to have originated from higher or lower trait values depending on the direction of the drift.

A.1 The effect of the mean drift: QBD3 model

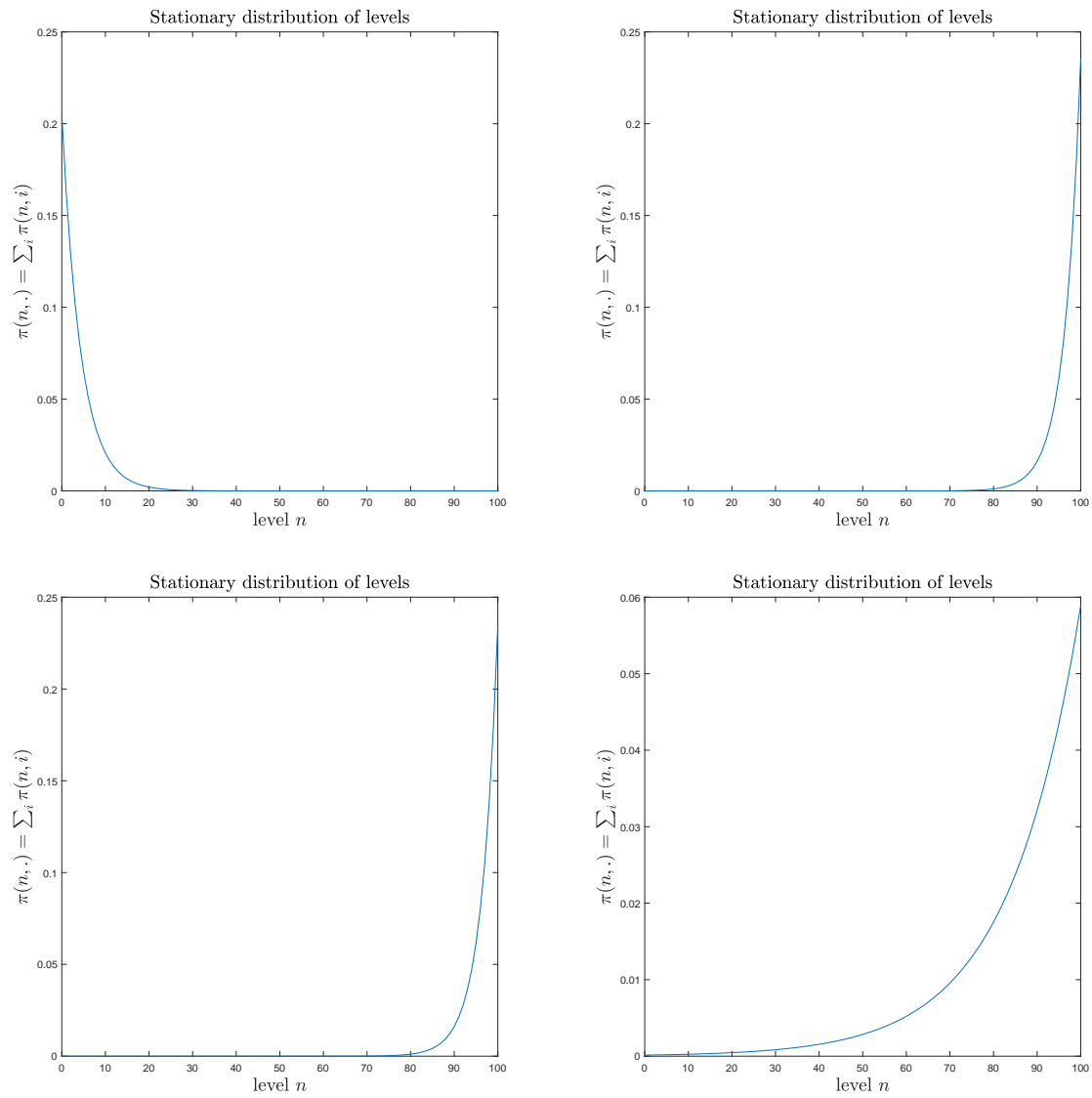


Figure 9: From top left to the bottom right: Stationary distribution of the levels in the QBD3 model in Section 4 for the \mathbf{r} vectors #1 – #4 in Table 2.

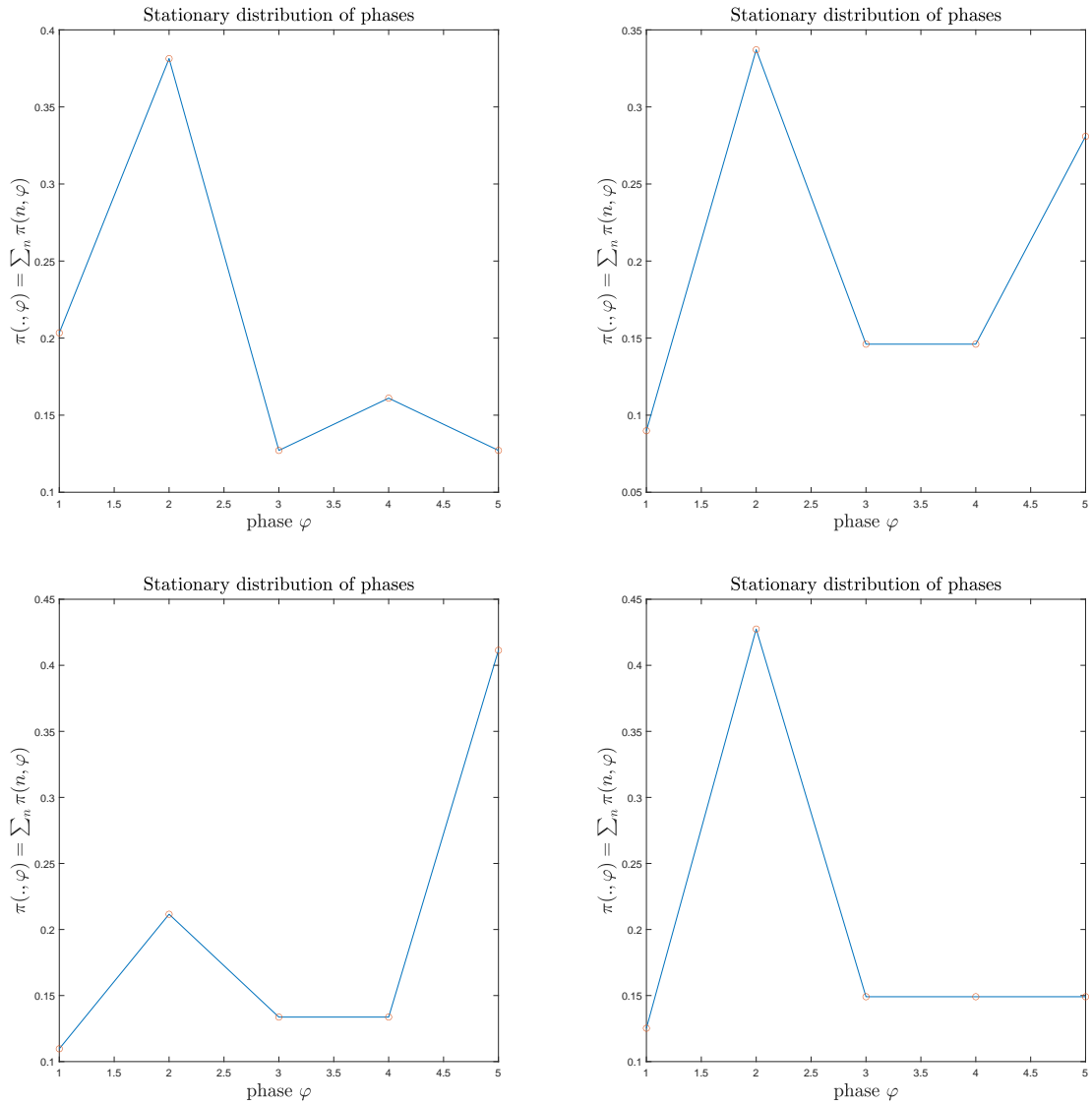


Figure 10: From top left to the bottom right: Stationary distribution of the phases $\varphi = 1, \dots, 5$ in the QBD3 model in Section 4 for the \mathbf{r} vectors #1 – #4 in Table 2.

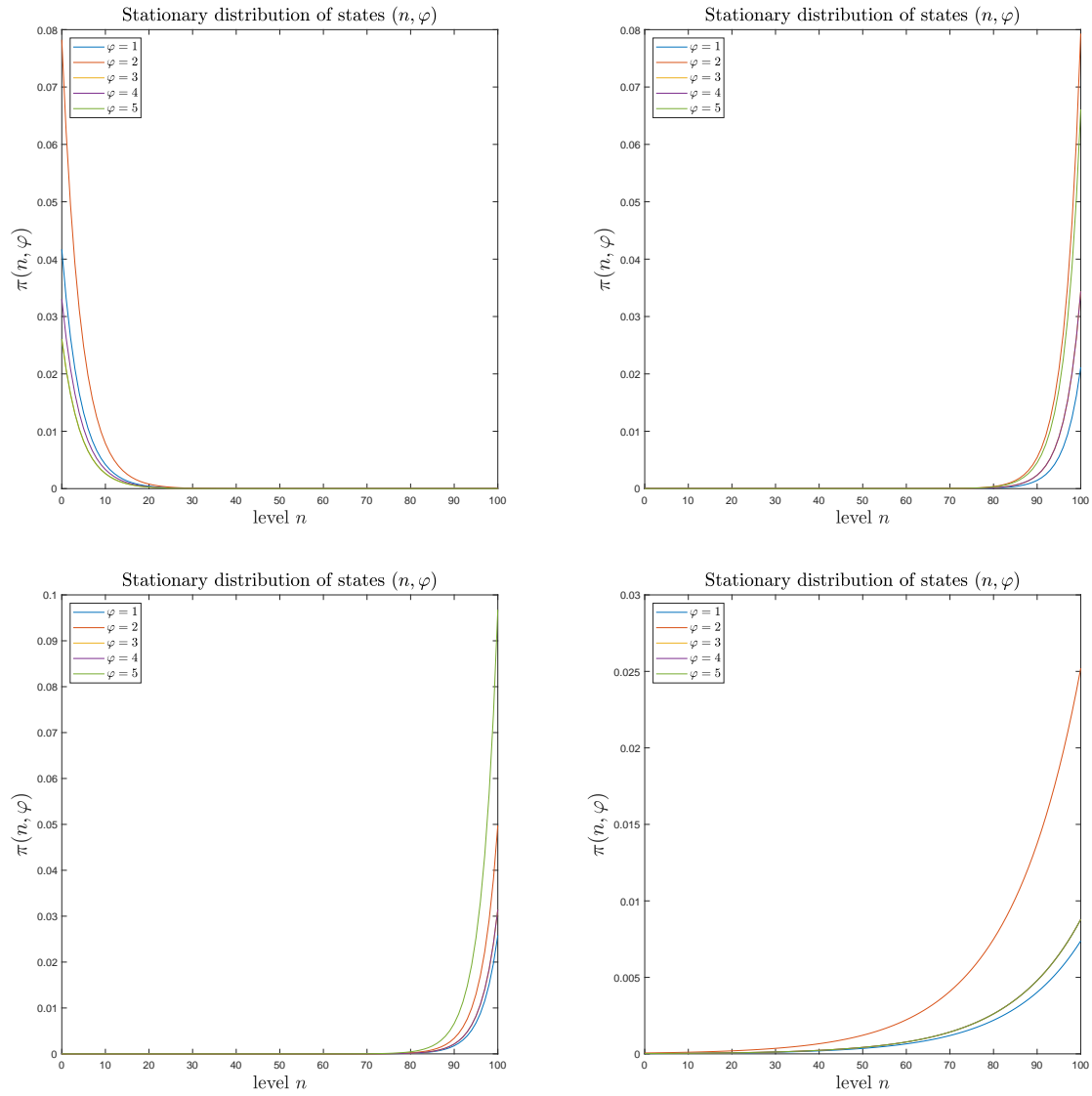


Figure 11: From top left to the bottom right: Stationary distribution of the states in the QBD3 model in Section 4 for the \mathbf{r} vectors #1 – #4 in Table 2.

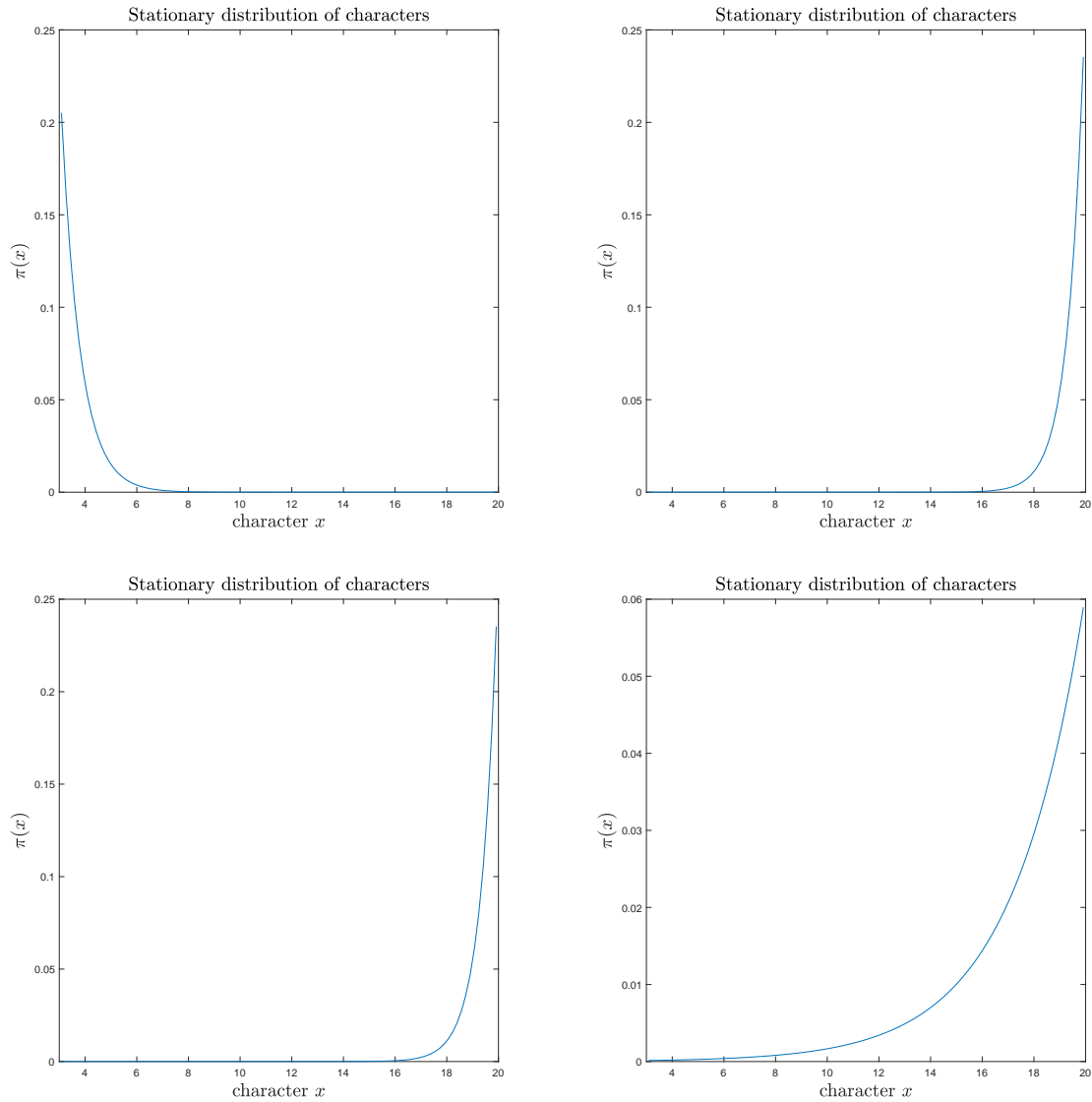


Figure 12: From top left to the bottom right: Stationary distribution of the traits in the QBD3 model in Section 4 for the \mathbf{r} vectors #1 – #4 in Table 2.

A.2 The effect of the mean drift: Synthetic Dataset 1 (Figure 3)

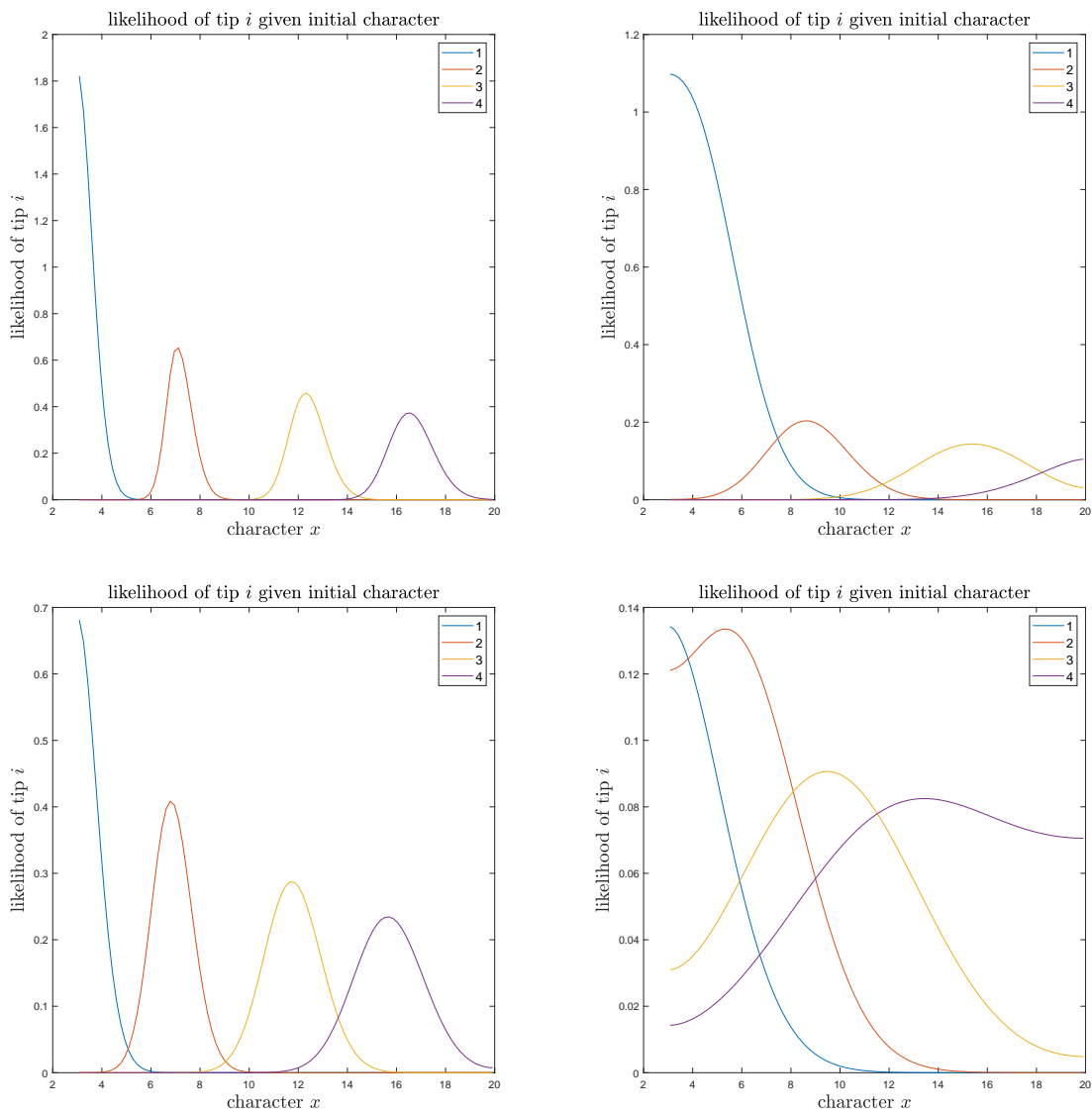


Figure 13: From top left to the bottom right: The likelihood of observing tip $i = 1, \dots, 4$ given trait observed at the start of the branch corresponding to tip i , in the QBD3 model in Section 4 and Synthetic Dataset 1 (Figure 3), for the \mathbf{r} vectors #1, #6, #4, and #9 in Table 2.

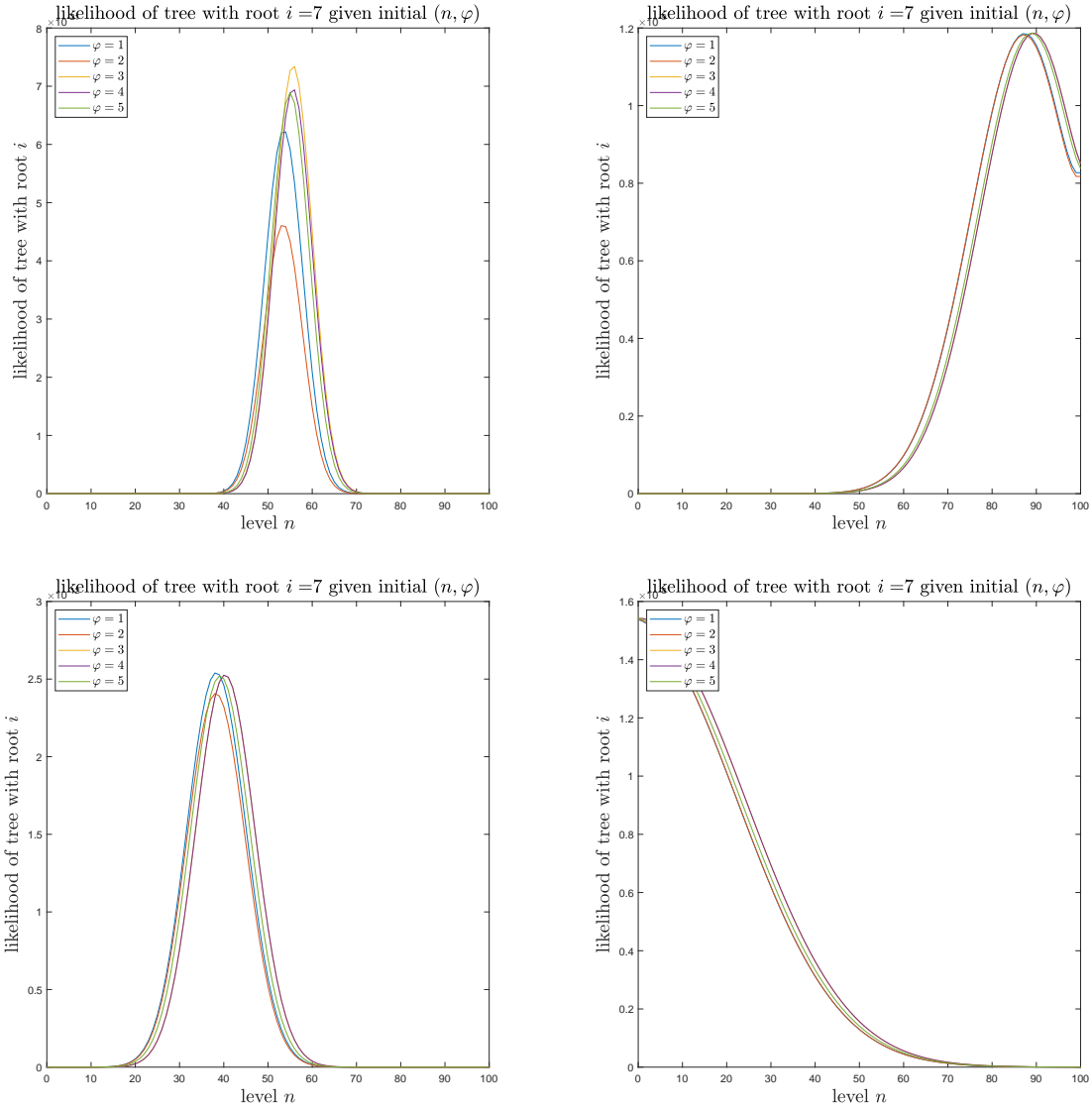


Figure 14: From top left to the bottom right: The likelihood of observing the phylogenetic tree that started with parent $i = 7$ given level n and phase φ observed at the start of the tree, in the QBD3 model in Section 4 and Synthetic Dataset 1 (Figure 3), for the \mathbf{r} vectors #1, #6, #4, and #9 in Table 2.

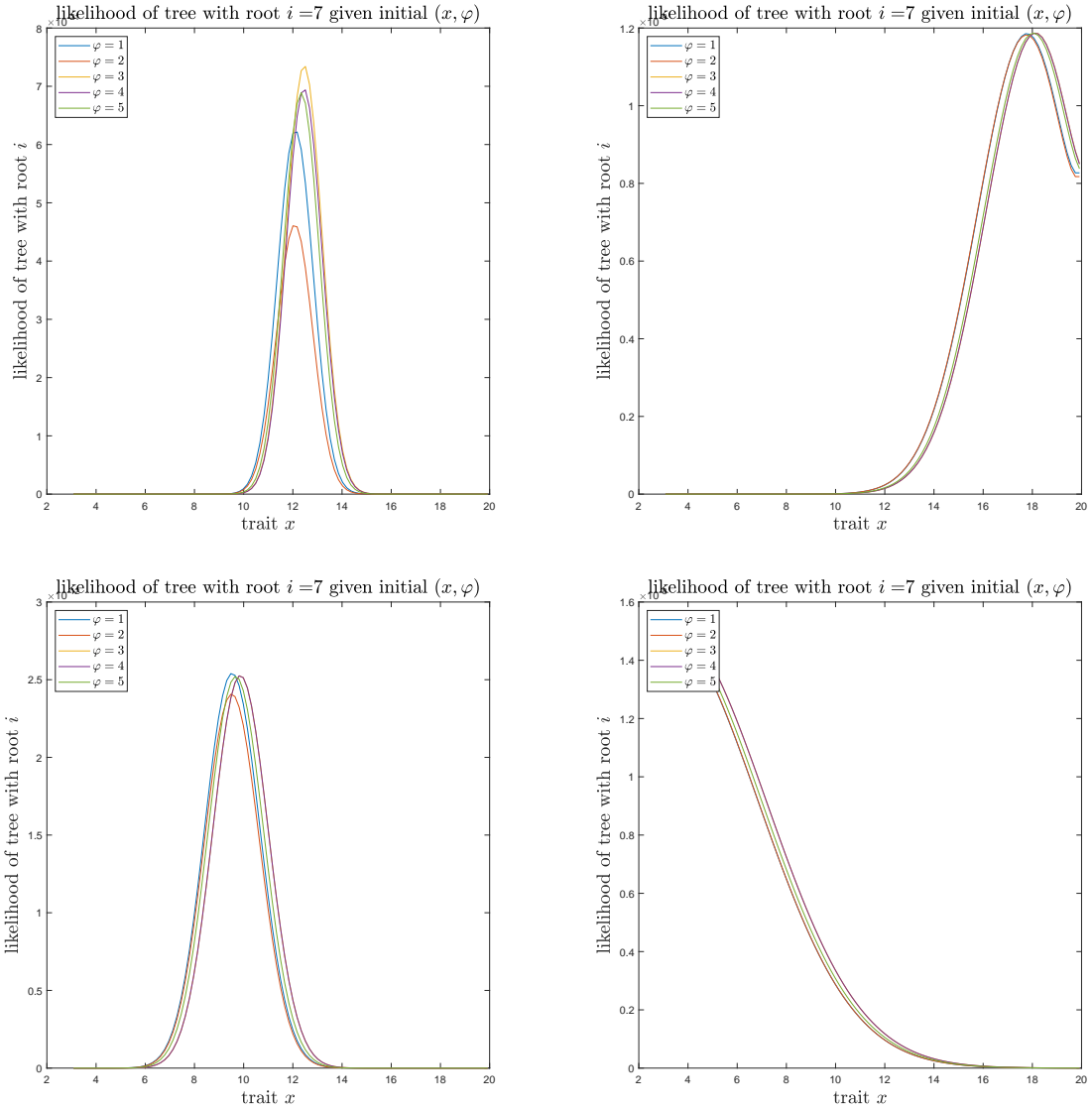


Figure 15: From top left to the bottom right: The likelihood of observing the phylogenetic tree that started with parent $i = 7$ given trait x and phase φ observed at the start of the tree, in the QBD3 model in Section 4 and Synthetic Dataset 1 (Figure 3), for the \mathbf{r} vectors #1, #6, #4, and #9 in Table 2.

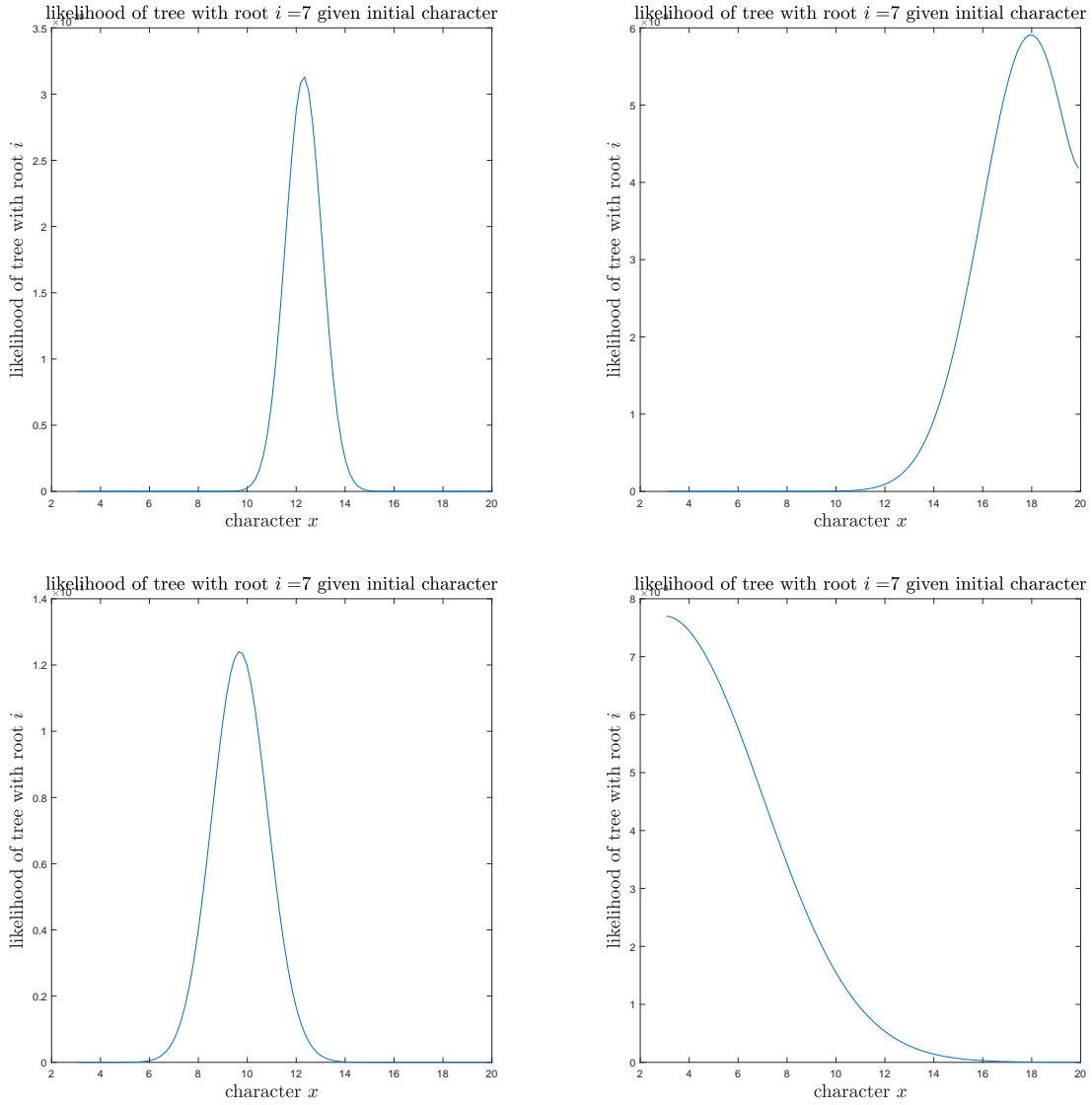


Figure 16: From top left to the bottom right: The likelihood of observing the phylogenetic tree that started with parent $i = 7$ given trait x observed at the start of the tree, in the QBD model in the QBD3 model in Section 4 and Synthetic Dataset 1 (Figure 3), for the \mathbf{r} vectors #1, #6, #4, and #9 in Table 2.

A.3 The effect of the mean drift: Synthetic Dataset 2 (Figure 4)

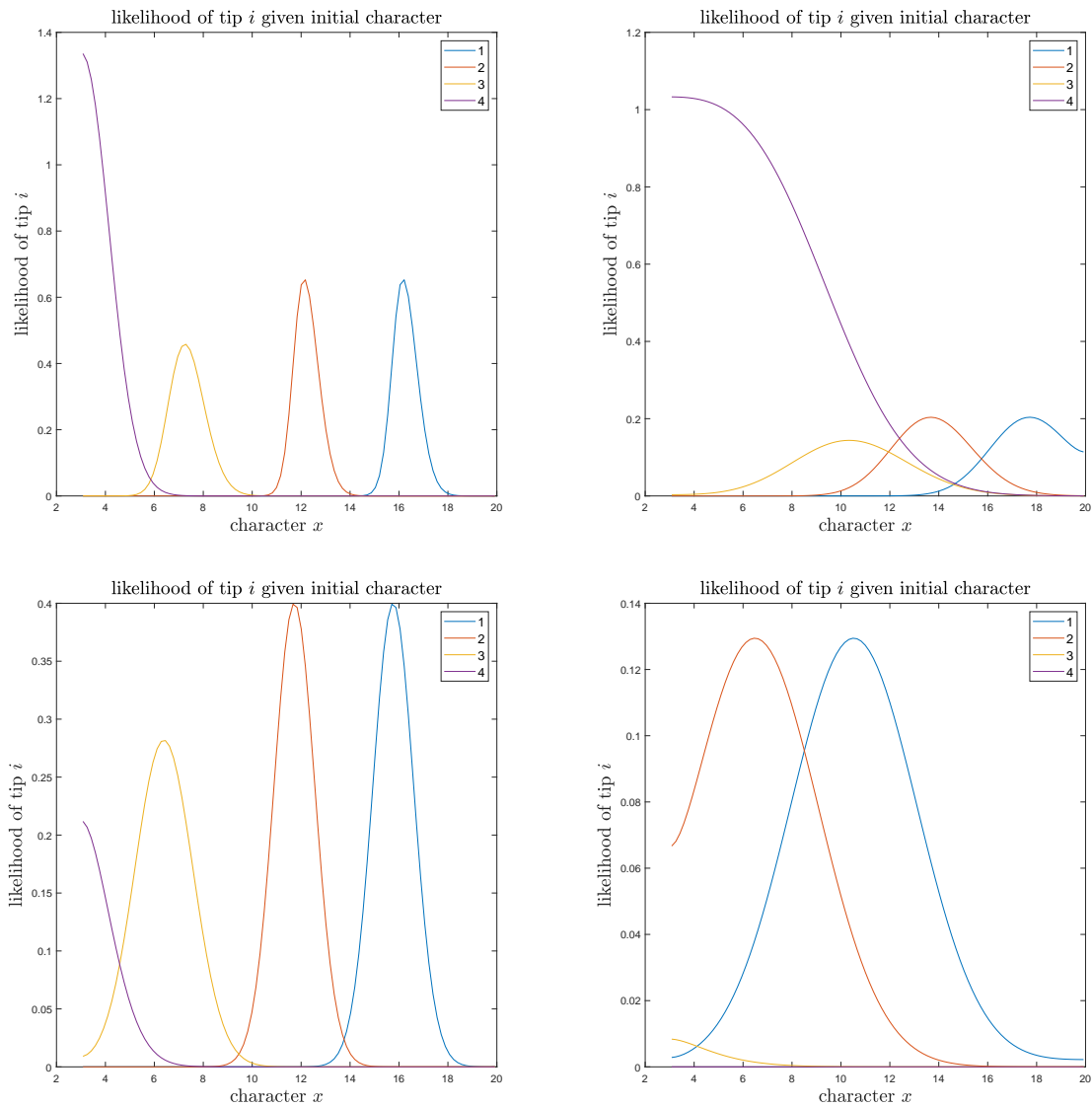


Figure 17: From top left to the bottom right: The likelihood of observing tip $i = 1, \dots, 4$ given trait observed at the start of the branch corresponding to tip i , in the QBD3 model in Section 4 and Synthetic Dataset 2 (Figure 4), for the \mathbf{r} vectors #1, #6, #5, and #8 in Table 6.

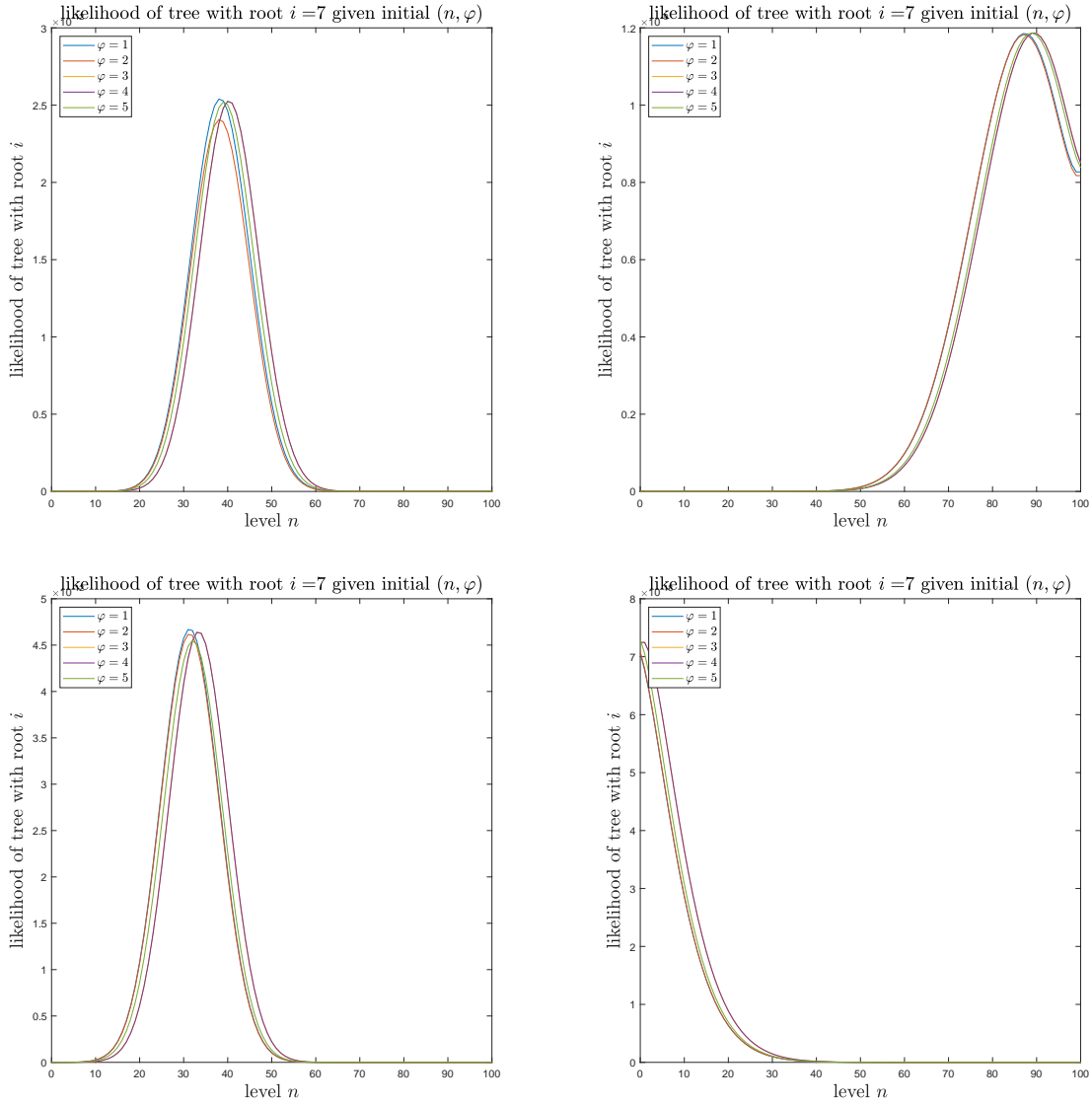


Figure 18: From top left to the bottom right: The likelihood of observing the phylogenetic tree that started with parent $i = 7$ given level n and phase φ observed at the start of the tree, in the QBD3 model in Section 4 and Synthetic Dataset 2 (Figure 4), for the \mathbf{r} vectors #1, #6, #5, and #8 in Table 6.

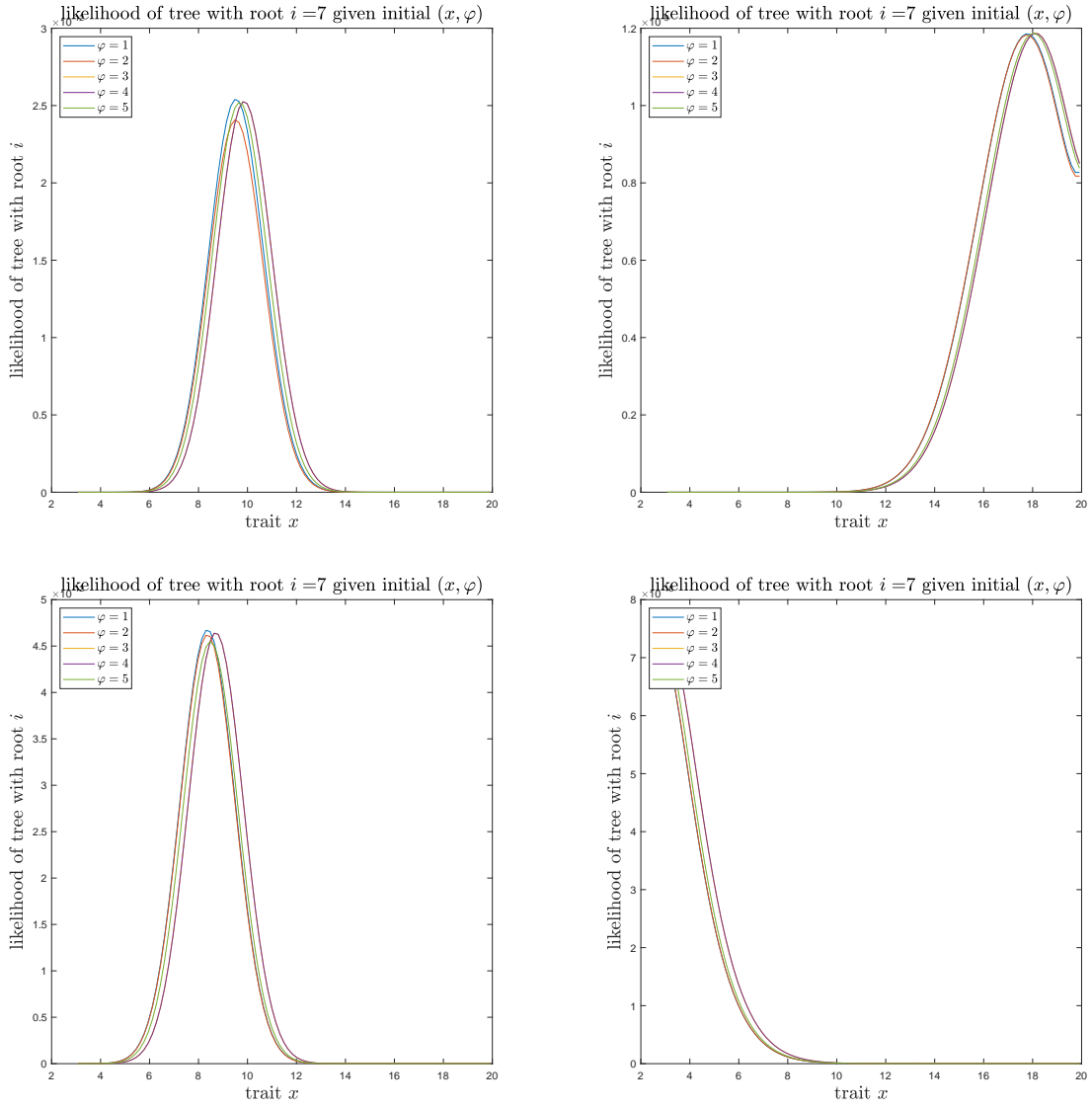


Figure 19: From top left to the bottom right: The likelihood of observing the phylogenetic tree that started with parent $i = 7$ given trait x and phase φ observed at the start of the tree, in the QBD3 model in Section 4 and Synthetic Dataset 2 (Figure 4), for the \mathbf{r} vectors #1, #6, #5, and #8 in Table 6.

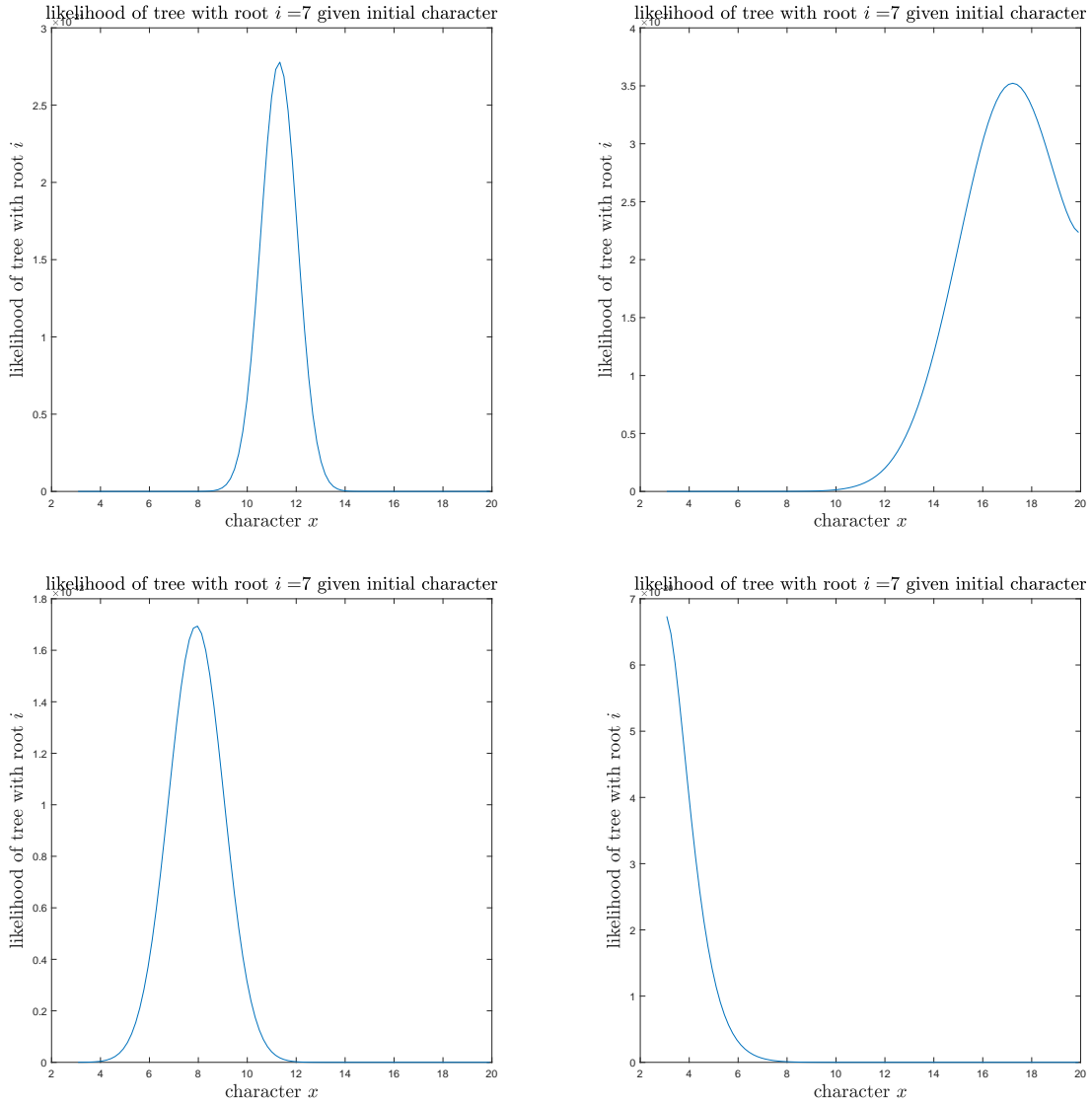


Figure 20: From top left to the bottom right: The likelihood of observing the phylogenetic tree that started with parent $i = 7$ given trait x observed at the start of the tree, in the QBD3 model in Section 4 and Synthetic Dataset 2 (Figure 4), for the \mathbf{r} vectors #1, #6, #5, and #8 in Table 6.

B Output: Empirical Dataset 1 (Figure 5)

Here, we consider the QBD3 model in Section 4 with five phases, and evaluate the likelihood of the Empirical Dataset 1 for a range of the QBD parameters.

We can see in Figure 21 that the 4 parameter sets with positive drift (\mathbf{r} vectors #2 – #5 in Table 10) give broadly similar sets of likelihood curves. Curves vary in their width depending on the height of the branch leading to tip i . It also seems that parameter sets with drift closer to zero produce broader curves whereas the two parameter sets with the largest (positive) drift have narrower curves centered around lower initial trait values.

In Figures 22, 23 and 24 we can again see that the behaviour seems to be dominated by the drift with the panels corresponding to \mathbf{r} vectors #2 – #5 all giving higher likelihood to root states where the level is near the lower boundary whereas panel one prefers root states with levels near the upper boundary.

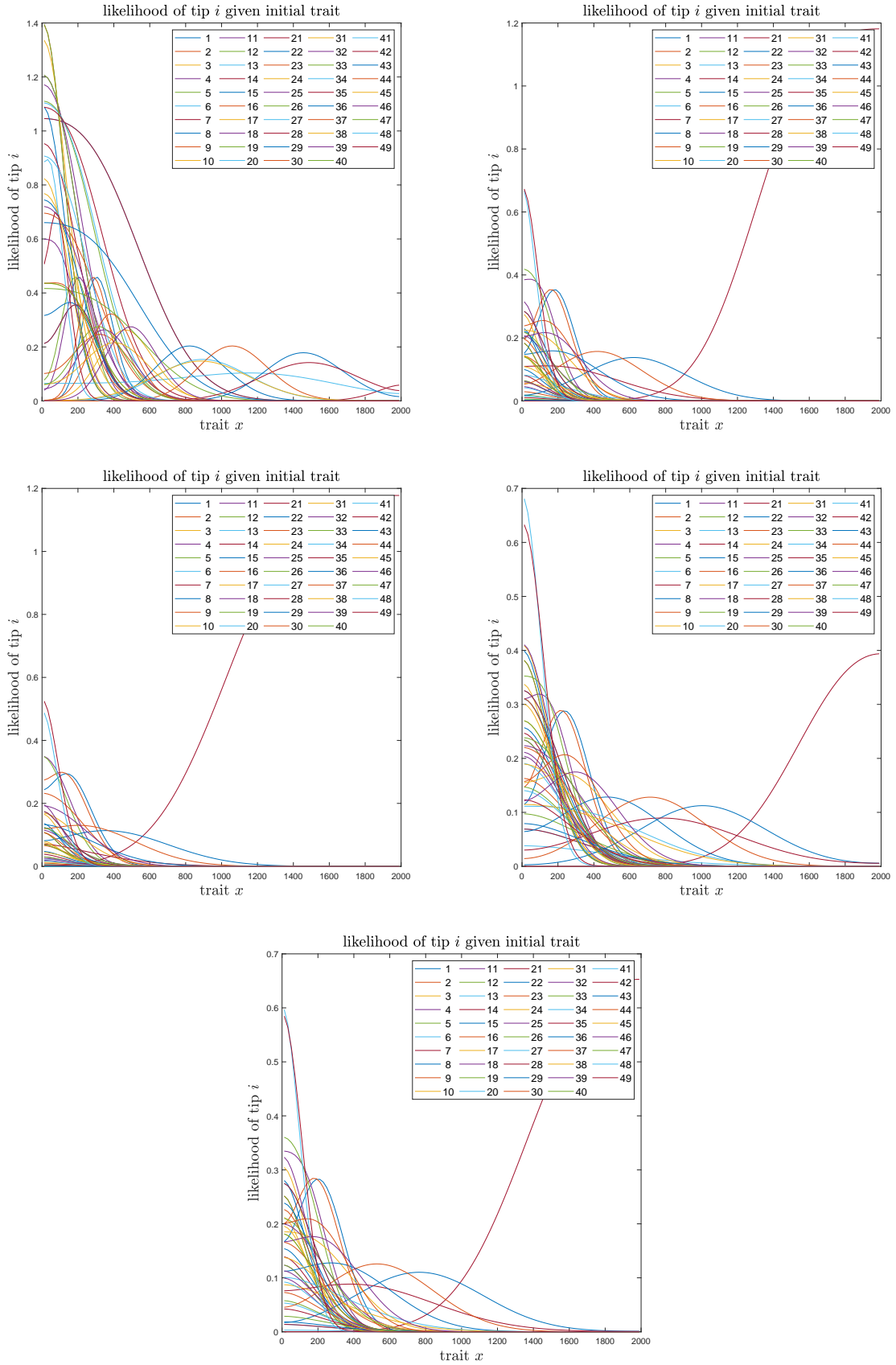


Figure 21: From top left to the bottom right: The likelihood of observing tip i given trait observed at the start of the branch corresponding to tip i , in the QBD3 model in Section 4 and Empirical Dataset 1 (Figure 5), for the \mathbf{r} vectors #1 – #5 in Table 10.

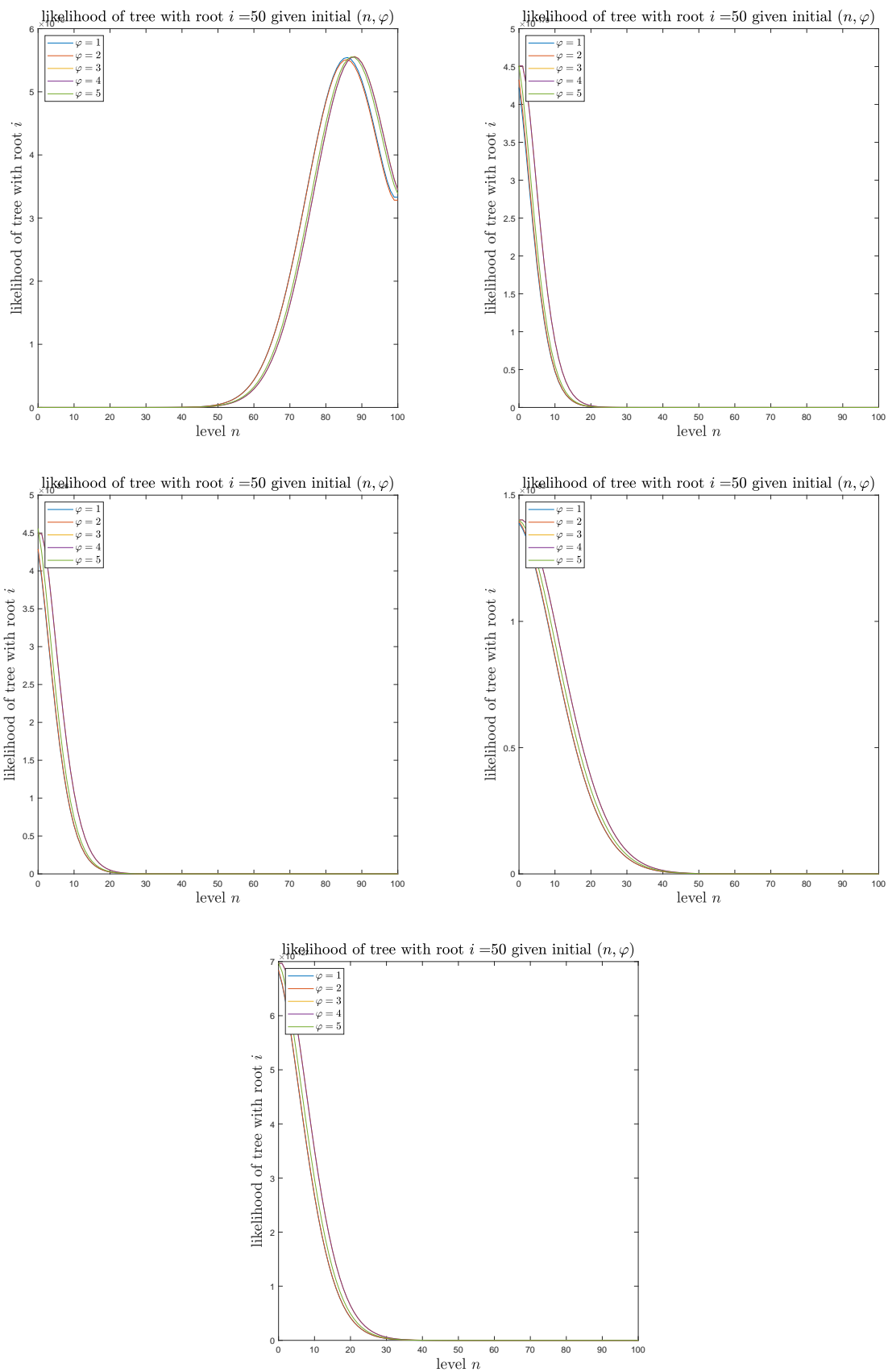


Figure 22: From top left to the bottom right: The likelihood of observing the phylogenetic tree that started with parent i given level n and phase φ observed at the start of the tree, in the QBD3 model in Section 4 and Empirical Dataset 1 (Figure 5), for the \mathbf{r} vectors #1 – #5 in Table 10.

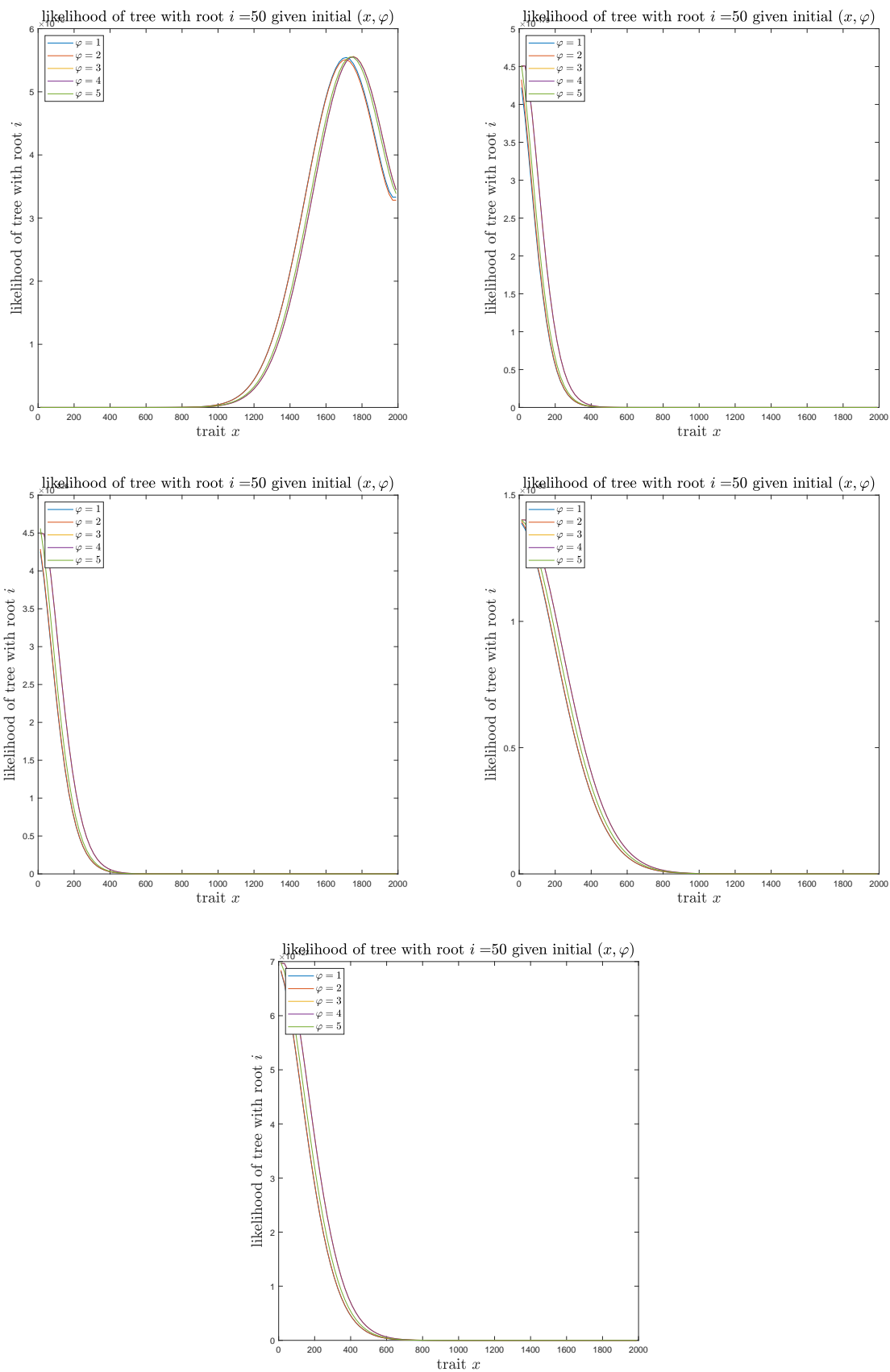


Figure 23: From top left to the bottom right: The likelihood of observing the phylogenetic tree that started with parent i given trait x and phase φ observed at the start of the tree, in the QBD3 model in Section 4 and Empirical Dataset 1 (Figure 5), for the \mathbf{r} vectors #1 – #5 in Table 10.

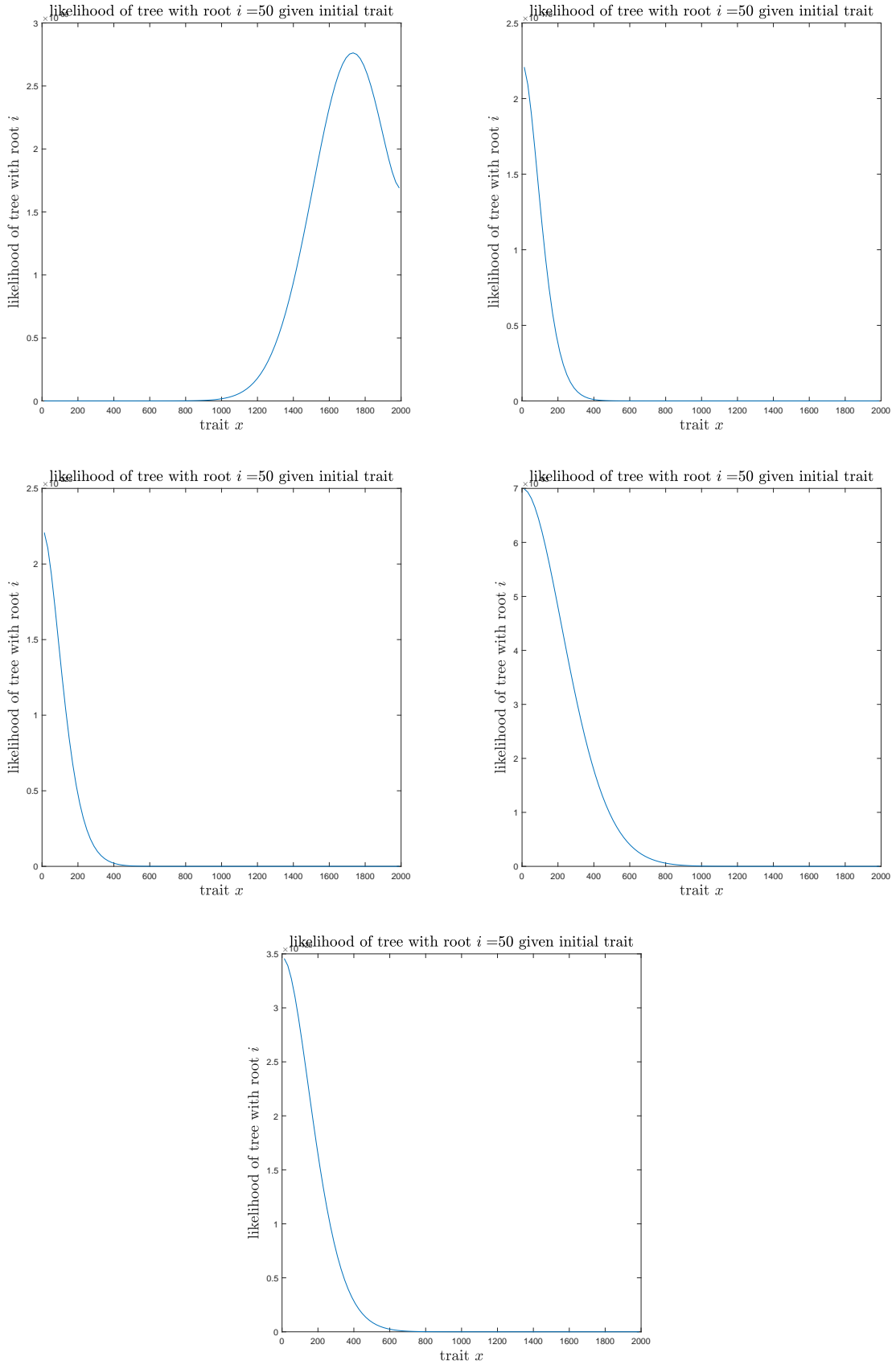


Figure 24: From top left to the bottom right: The likelihood of observing the phylogenetic tree that started with parent i given trait x observed at the start of the tree, in the QBD3 model in Section 4 and Empirical Dataset 1 (Figure 5), for the \mathbf{r} vectors #1 – #5 in Table 10.

C Output: Empirical Dataset 2 (Figure 7)

Here, we consider the QBD3 model in Section 4 with five phases, and evaluate the likelihood of the Empirical Dataset 2 for a range of the QBD parameters.

We can see in Figure 25 that the 4 parameter sets with positive drift (\mathbf{r} vectors #2 – #5 in Table 10) give broadly similar sets of likelihood curves. Curves vary in their width depending on the height of the branch leading to tip i . It also seems that parameter sets with drift closer to zero produce broader curves whereas the two parameter sets with the largest (positive) drift have narrower curves centered around lower initial trait values.

In Figures 26, 27 and 28 we can again see that the behaviour seems to be dominated by the drift with the panels corresponding to \mathbf{r} vectors #2 – #5 all giving higher likelihood to root states where the level is near the lower boundary whereas panel one prefers root states with levels near the upper boundary.

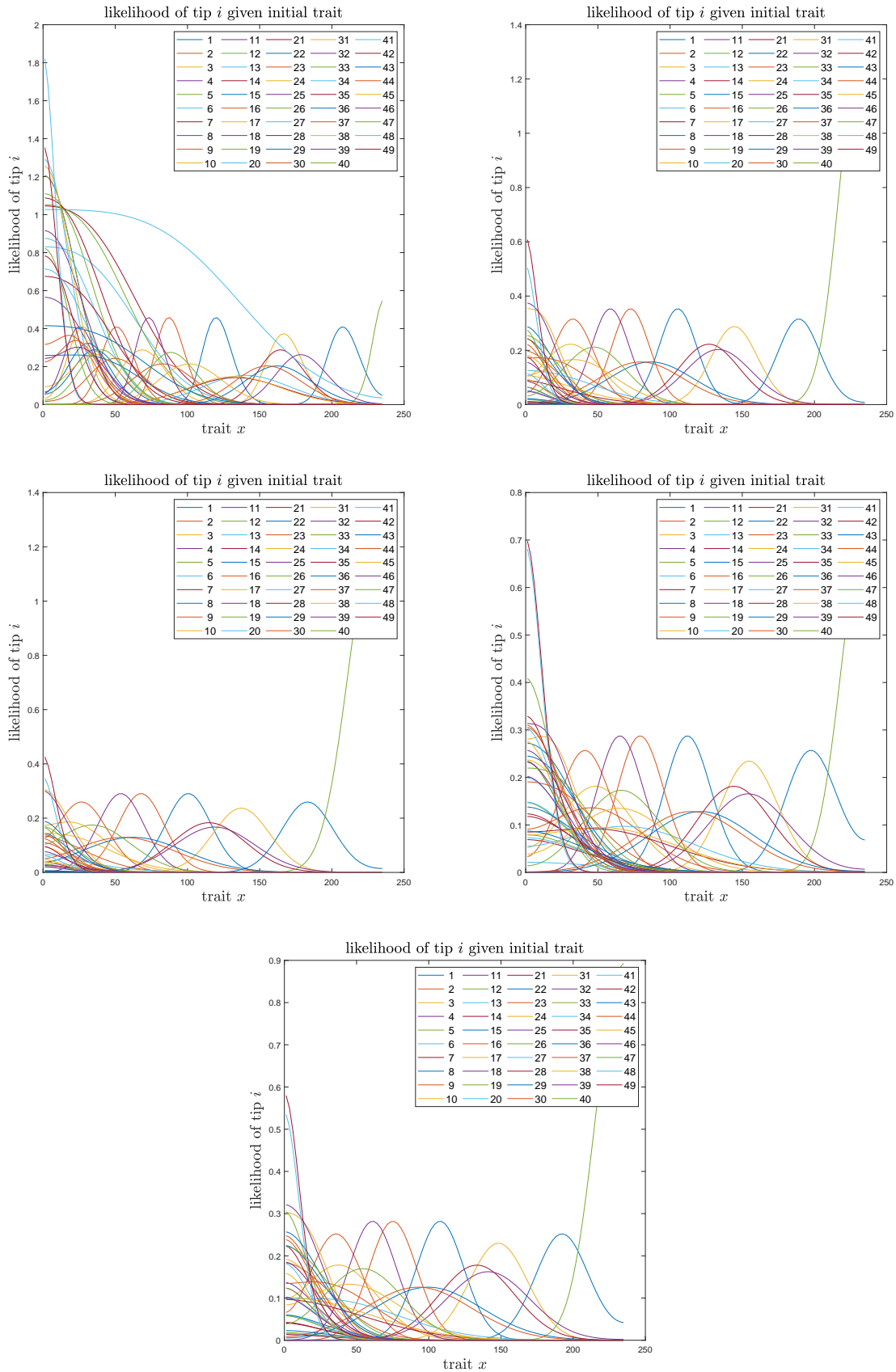


Figure 25: From top left to the bottom right: The likelihood of observing tip i given trait observed at the start of the branch corresponding to tip i , in the QBD3 model in Section 4 and Empirical Dataset 2 (Figure 7), for the \mathbf{r} vectors #1 – #5 in Table 13.

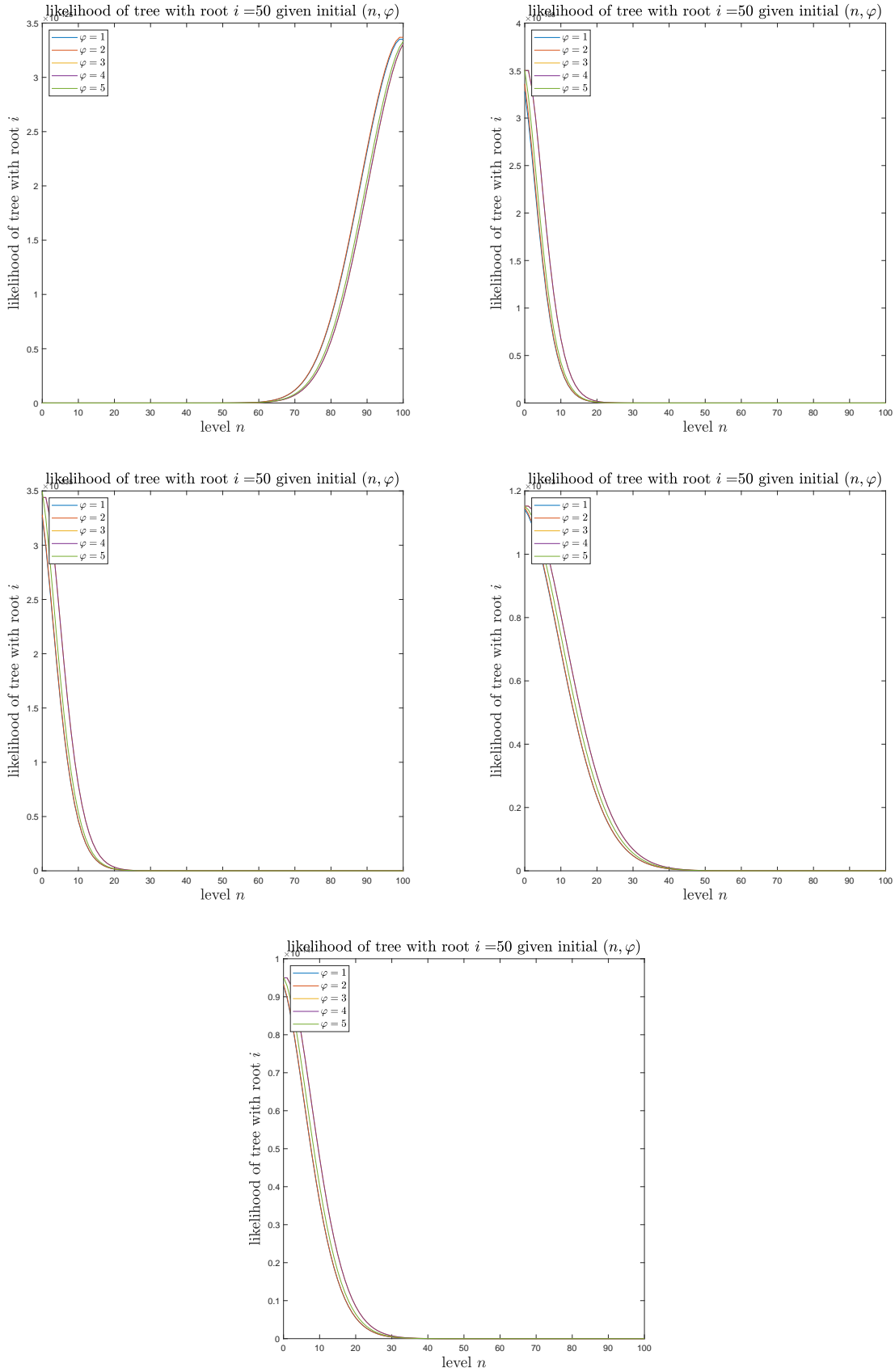


Figure 26: From top left to the bottom right: The likelihood of observing the phylogenetic tree that started with parent i given level n and phase φ observed at the start of the tree, in the QBD3 model in Section 4 and Empirical Dataset 2 (Figure 7), for the \mathbf{r} vectors #1 – #5 in Table 13.

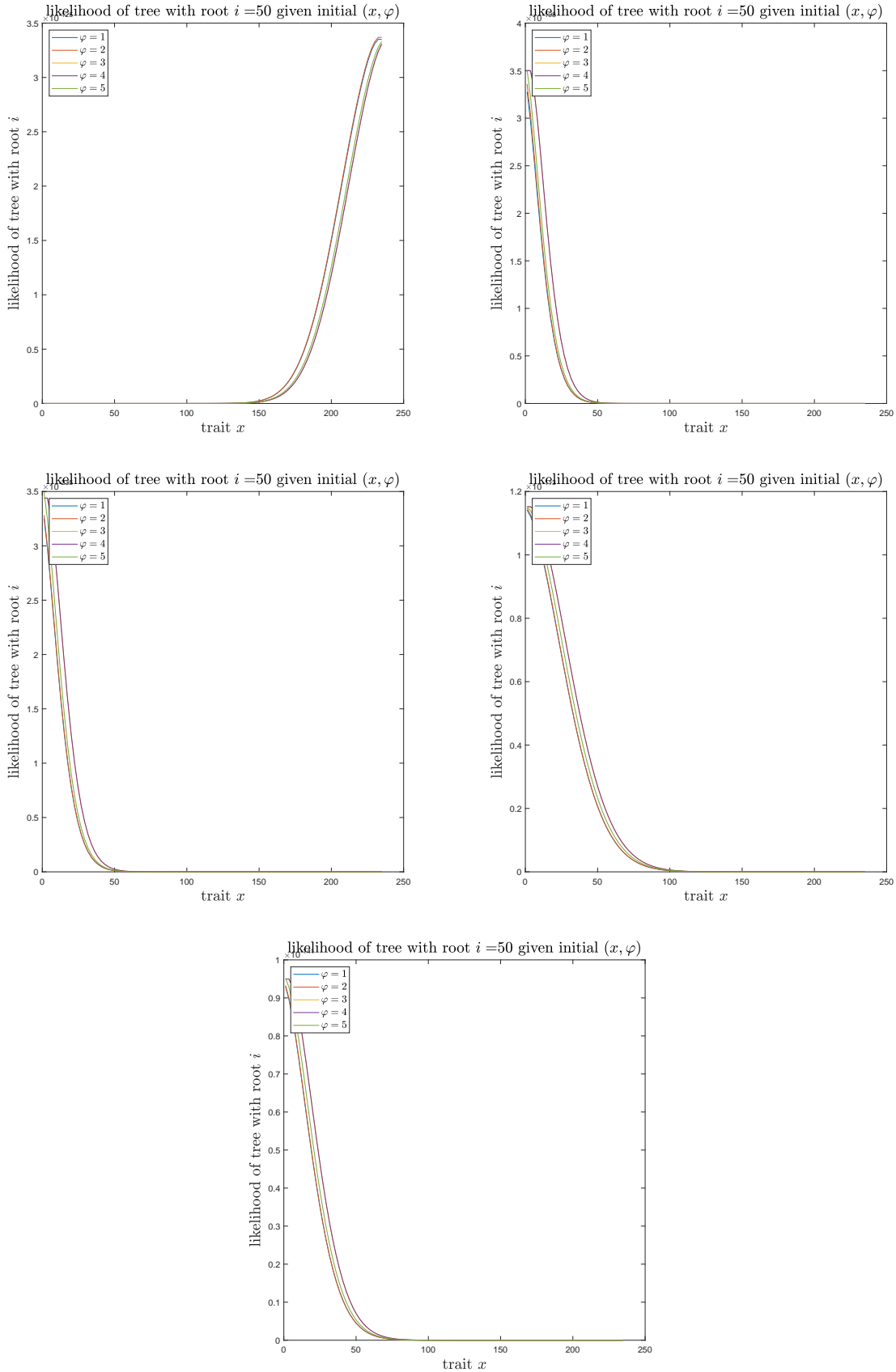


Figure 27: From top left to the bottom right: The likelihood of observing the phylogenetic tree that started with parent i given trait x and phase φ observed at the start of the tree, in the QBD3 model in Section 4 and Empirical Dataset 2 (Figure 7), for the \mathbf{r} vectors #1 – #5 in Table 13.

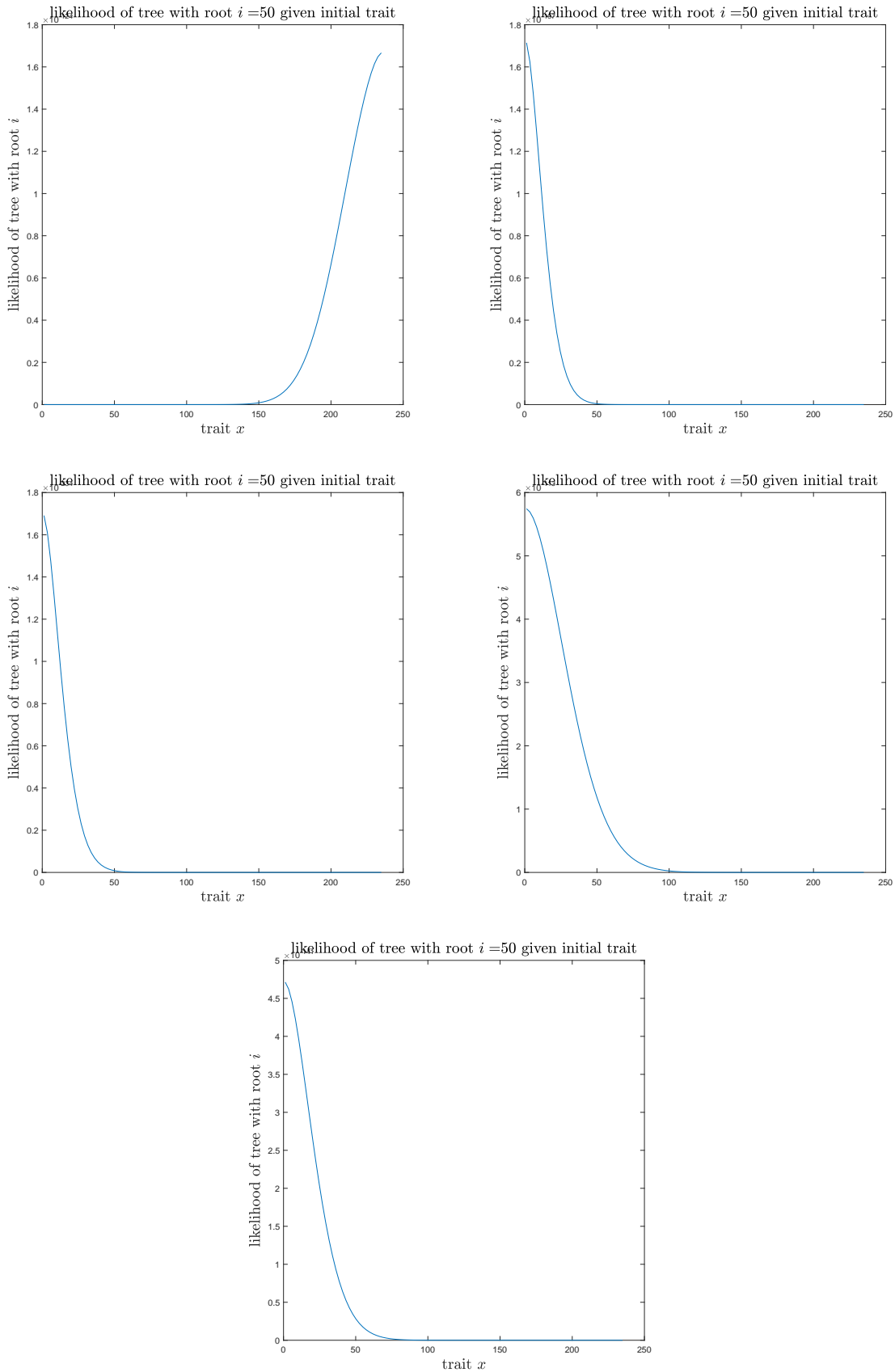


Figure 28: From top left to the bottom right: The likelihood of observing the phylogenetic tree that started with parent i given trait x observed at the start of the tree, in the QBD3 model in Section 4 and Empirical Dataset 2 (Figure 7), for the \mathbf{r} vectors #1 – #5 in Table 13.